Available online at www.CivileJournal.org

Civil Engineering Journal

(E-ISSN: 2476-3055; ISSN: 2676-6957)

Vol. 9, No. 05, May, 2023

Shear Behavior of Reinforced Concrete Inverted-T Deep Beam

Hoda Shousha [1*], Rasha T. S. Mabrouk [1], Akram Torkey [1]

[1] *Structural Engineering Department, Faculty of Engineering, Cairo University, Giza, Egypt.*

Received 04 February 2023; Revised 15 March 2023; Accepted 29 March 2023; Published 01 May 2023

Abstract

Contrary to top-loaded deep beams, Inverted-T (IT) deep beams are loaded on ledges at the beam's bottom chord. The presence of the load near the bottom of the beams creates a tension field in the web at the loading points. An experimental investigation was carried out in which 8 specimens of reinforced concrete IT deep beams were tested and the effect of the following variables was studied: changing the hanger diameter, hanger arrangement in terms of spacing and distribution distance, hanger reinforcement ratio, vertical and horizontal web shear reinforcement diameter, and spacing. In addition, all the tested beams had long ledges extending to the end of the beam. It was concluded that hanger reinforcement diameter and horizontal web shear reinforcement have an insignificant effect on the IT deep beam capacity. While the change in hanger arrangement, vertical web reinforcement, and ledge length has a significant effect on IT deep beam capacity. The maximum spacing of the hanger reinforcement and the minimum hanger reinforcement ratio passing through the load plate length will be studied in the following publication. A finite element model (FEM) was presented to predict the behavior of IT deep beams. The simulation was carried out using the ABAQUS 2017 software program. The results of the numerical model showed good agreement with the experimental program. Analysis using design codes was checked against the experimental data, where the computed beam capacities were compared to those obtained from the test results. The comparison showed a remarkable difference between the predictions using the design codes and the test results. Computation using design codes significantly underestimated the capacities of the beams.

Keywords: Type Inverted-T Beam; Finite Element; Shear; Hanger; Reinforcement; Ledge.

1. Introduction

Reinforced concrete inverted-T (IT) deep beams provide a popular and natural structural form for use as a girder supporting precast members. It is commonly used in most special structures that sustain heavy loads, such as bridges and high-rise buildings. The ledge of the inverted-T deep beams acts as a shallow shelf supporting precast beams while the stem rises to the supported beam height, providing the required depth to sustain shear and flexure forces. Figure 1a shows how the use of inverted T-beams increases the clearance underneath the bridge deck while still maintaining an attractive appearance by minimizing the visible size of transverse supporting members. In large-span slabs, IT beams are usually used to support precast hollow core slabs and double T slabs, as shown in Figures 1b and 1c.

IT deep beams have different structural behavior than the more conventional top-loaded deep beams as the load transfers from the ledges to the bottom of the web, then "hung" vertically to the compression chord, forming tension fields in the web at the load location as shown in Figure 2. The loads are then transmitted longitudinally to the supports, as in a typical top-loaded deep beam.

* Corresponding author: hoda1510362@eng1.cu.edu.eg

http://dx.doi.org/10.28991/CEJ-2023-09-05-04

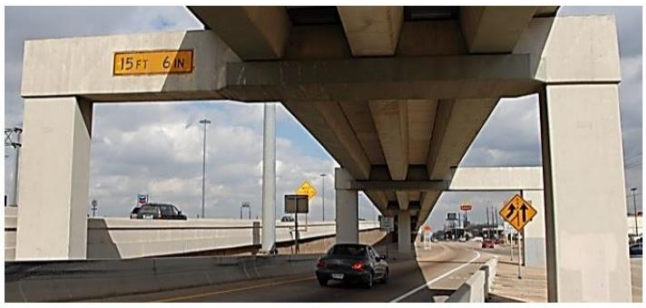

(a)

(b)

(c)

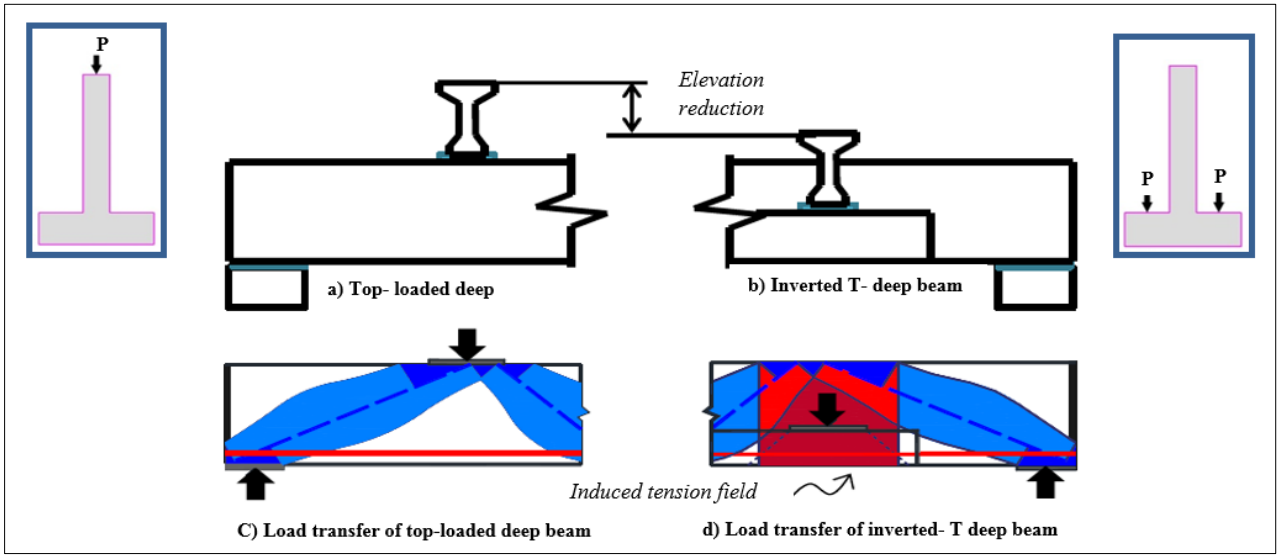

Figure 1. Typical inverted-T deep beams

Figure 2. Load transfer of top-loaded deep beam vs. inverted T-deep beam

1.1. Codes' Definition of Deep Beams

Both ECP 203-2020 [1] and ACI 318-19 [2] stated that deep beams are members with one loaded face and supported on the opposite face, allowing compression struts to form between the loads and the supports and having clear spans equal to or less than four times the member depth, while the deep beam in EN 1992-1-1 [3] is defined as a member with a span that is less than three times the section depth. Figure 3 shows the main components of the IT deep beam.

Before establishing the experimental investigation, a thorough literature review was carried out. Researchers [4–11] have studied the shear behavior of IT deep beams since the 1940s. Based on the test data, the effect of the following parameters was evaluated: longitudinal reinforcement ratio, shear span to depth ratio, and the amount and configuration of web reinforcement.

In 1943, Graf et al. [4] tested one tension-chord-loaded specimen. The load was applied through horizontal nips built into the soffit. The hanger reinforcement stopped at the mid-height of the IT deep beam. The failure occurred as a result of the main reinforcement yielding and the deterioration of the section directly above the horizontal nips.

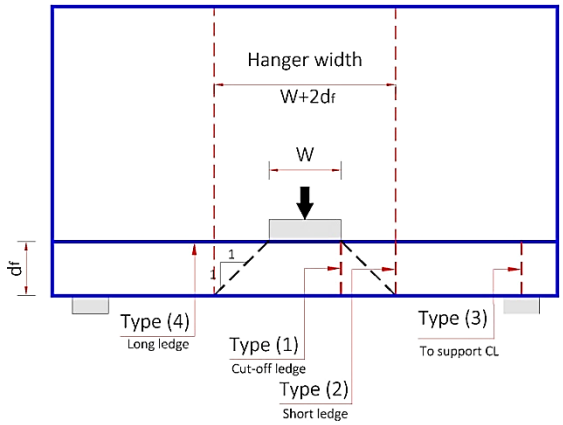

(a) Ledge types and hanger width

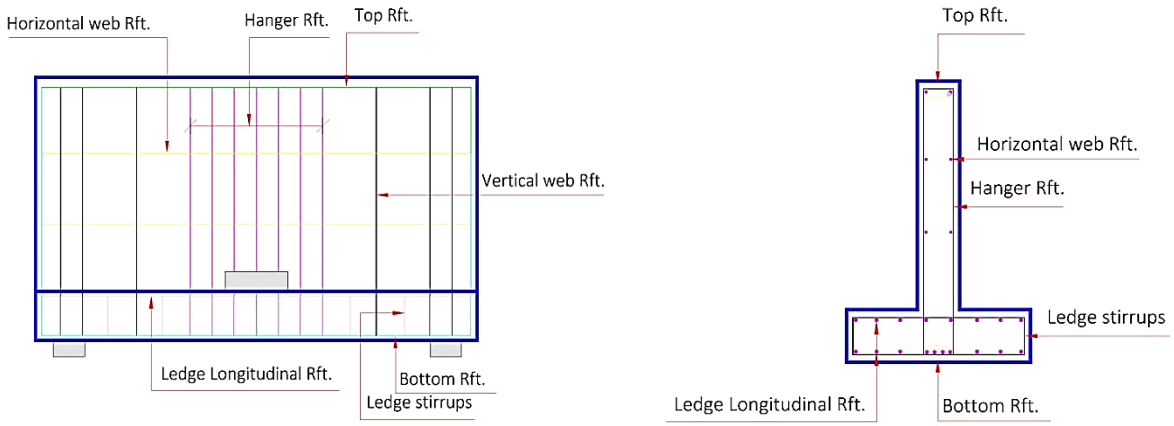

(b) Reinforcement details

Figure 3. Inverted T-deep beam components

In 1966, Leonhardt et al. [5] tested four tension-chord-loaded specimens. It was concluded that the optimal methods of providing main reinforcement were using well-anchored bars as support and horizontal hooks for anchoring. It was also recommended that the main reinforcement be distributed across the bottom 20% of the beam height. It was suggested that stirrups be extended at a height equal to the span. Closely spaced (<400mm) stirrups were suggested to decrease crack widths, with vertical stirrups covering the whole height of the beam.

Furlong et al. (1971) [6] and Mirza et al. (1988) [7] tested two full-scale and four one-third-scale specimens to study ledge and web shear reinforcement of the inverted T cross-section. Some specimens were loaded on both chords simultaneously. Open stirrups were used in some of the specimens. The findings provide advice for hanger reinforcement. It was also recommended that hanger stirrups be closed at the bottom. It was concluded that it is not necessary to superimpose loads on stirrups acting as hangers and loads on stirrups acting as shear reinforcement. The width of the bracket that can be considered effective in flexure and the reinforcement were also presented in this study. In 1974 and 1985, Furlong et al. and Mirza & Furlong [8, 9] recommended design procedures and formulas for determining hanger strength and serviceability requirements and the required flange thickness to resist punching. Other recommendations for designing flange transverse reinforcement in prestressed or non-prestressed beams were proposed. Supplementary guidelines for designing stirrups and defining ledge depth requirements were also presented.

Smith & Fereig (1974) [10] tested four tension-chord-loaded specimens. Specimens were indirectly supported on both ends of the beam. The effect of web reinforcement on ultimate capacity was studied, and it showed that web reinforcement has a significant effect on beam capacity. A comparison between the ultimate capacity of top- and bottom-loaded deep beams was investigated. The comparison showed that the crack width, steel strain, and deflection are higher in bottom-loaded deep beams. However, both types can sustain the same load if adequate vertical steel is located at the load location in the bottom-loaded deep beam. In 1977, Smith & Fereig [11] tested two tension-chord-loaded specimens (indirect loading). A study of the influence of loading and supporting conditions on the ultimate shear strength and the behavior of beams with short shear spans was provided. Tension-chord-loaded specimens exhibit a much smaller gain in strength by reducing the shear span-to-depth ratio than top-loaded beams, and the increase only occurs in the case of a shear span-to-depth ratio lower than 1.5. The addition of web reinforcement to the short shear span beams decreased crack widths, tensile steel strains, and deflections in general, but for the used reinforcement ratios, there was only a minor effect on the ultimate capacity of the directly loaded beams compared with a considerable strength contribution in the indirect case.

Cussens & Besser (1985) [12] tested five tension-chord-loaded specimens. The vertical reinforcement ratio was changed, and the effects on crack formation and ultimate shear capacity were investigated with the design recommendations of the American Concrete Institute and the Construction Industry Research and Information Association. In 1997, Tan et al. [13] tested six tension-chord-loaded specimens. Specimens had two load points. Two types of web reinforcement were investigated. The web reinforcement was detailed according to the recommendations of the UK CIRIA Guide 14. It is found that the CIRIA [14] detailing rules help to ensure ductility in the behavior of the specimens, and this, in turn, yields consistent ultimate shear strengths irrespective of the loading condition imposed on the beams. Comparisons with test results also show that the CIRIA predictions are both conservative and consistent.

The most recent and important experimental studies were conducted by Fernandez Gomez (2012) [15] and Varney et al. (2015) [16], in which thirty-three tests were performed on large-scale reinforced concrete IT deep beams. Five parameters were examined, as follows: (1) The length of the ledge (Type 1- cut-off, Type 2- short, and Type 3-up to the center line of the support as shown in Figure 3); (2) the ledge depth; (3) the amount of web reinforcement; (4) the number of loading points on the ledge, and (5) the web depth. The results showed that increasing the ledge length enhances the overall strength of the inverted-T deep beam and delays the formation of the first diagonal crack. Shear strength was found to be the lowest for specimens with cut-off ledges, while long ledges generally resulted in higher strength as well as diagonal cracking loads. The effect of ledge length on the increase in beam capacity will be studied in clause 7. It was also proposed by Fernandez Gomez [15] that the strut's weakest point for beams with long ledges may shift from the strut-to-node interface to the position where the thickness of the strut varies from the ledge width to the web width. This proposal will be verified in clause 6. The results also indicated that the strength of the inverted-T beams is not significantly affected by increasing the ledge depth. However, it was found that increasing the depth of the ledge could delay the formation of the first diagonal crack. It was also observed that increasing the web reinforcement ratio, increases the shear strength of inverted-T beams. The reinforcement ratio had minimal influence on the diagonal cracking load. It was found that a higher web reinforcement ratio was more effective in limiting the widths of the diagonal cracks. Consequently, at a given crack width, inverted-T beams with a larger web reinforcement ratio are more likely to be closer to their ultimate capacity than those with a lower ratio. AASHTO LRFD-2020's [17] minimum reinforcement ratio of 0.3% in each orthogonal direction for effective crack width control in rectangular deep beams was also determined to adequately restrain cracks at service loads in inverted-T beams. The test results also showed that the number of loading points has an insignificant influence on the capacity and the formation of the first diagonal crack. As loads increased, no change in the crack distribution or crack width progression was noticed in inverted-T beams. The strength and serviceability of the inverted T beams were not significantly affected by the change in web depth. A minor but otherwise negligible reduction in the first cracking load was detected.

Garber et al. (2017) [18] studied the behavior of IT deep beams experiencing ledge failures. It was concluded that either a 45-degree load-dispersion line extending from the ends of the bearing or the AASHTO [17] empirical approach can be used to determine the amount of hanger and ledge reinforcement that is engaged. Also, it was found that hanger reinforcement in IT deep beams contributes to both the sectional shear strength and the transfer of load from the ledge up into the compression chord within the beam. Moreover, the use of STM also allowed for the capacity of the ledge to be estimated in a more straightforward manner than the AASHTO empirical method [17]. Both methods will be evaluated later in this paper. Rai (2021) [19] investigated a numerical modeling technique to study the nonlinear behavior of RC deep beams by using FEA based on the software ABAQUS [20]. The response of the FE model is verified with the experimental results in terms of the load-to-midspan deflection curve and damage distribution. The ultimate shear capacity predicted by the FE model is 0.75% lower, and the corresponding displacement is 6.92% higher than the experimental results.

Ali et al. (2023) [21] investigated numerically the overall behavior of simply supported concrete deep beams reinforced with and without carbon fiber-reinforced polymer (CFRP) sheets through forty. It was concluded that the simulated configurations of failure modes in the FE model (ABAQUS) are consistent with the experimental findings. A comparison between the load-deflection curves of the modeled members versus the corresponding experimental ones showed that the predicted load-deflection curve is relatively similar to the experimental curves. It concludes that the chosen FE model and inputs are capable of providing reliable results and can be further used to evaluate the failure mechanism of deep beam specimens.

From the literature, it can be seen that the majority of the specimens were found to give unrealistic results or didn't fulfill the definition of the deep beam. A significant number of specimens had an aspect ratio (L/d) of more than 4, and some have a depth that is more than 12 times their width. Such a high ratio is impractical for deep beams and contradicts the provisions of the relevant codes, such as ECP 203-2020 [1], ACI 318-19 [2], and Eurocode 2 [3]. Some of the specimens did not fail to the end of experiments 6, 12, noting that ultimate capacity information is necessary to assess specimens' performance. Other specimens were tested with combined tension- and compression-chord loading [12]. This condition is not typical of field specimens that do not experience heavy loads on both chords. No shear reinforcement was used in some specimens, which is an impractical condition because in-service beams normally have

a minimum amount of transverse reinforcement. Plate size information was incomplete in some specimens. Other specimens had complicated geometry, support conditions, or reinforcement details, leading to unrealistic conditions when compared to in-service beams. Figure 4 shows samples of the unrealistic support conditions and reinforcement details found in the literature. In addition, previous research focused mainly on the size and geometry of the IT deep beams. Even the effect of web shear reinforcement was studied in most research for both vertical and horizontal reinforcement simultaneously. The hanger reinforcement was arranged in most cases based on the 45-degree concept of load spreading proposed by the codes without considering the effect of hanger reinforcement diameter, ratio, and arrangement on the strength of the IT deep beam. All the experiments were performed on specimens with a ledge of types 1, 2, and 3, as shown in Figure 3a. The case of a beam with a long ledge (type 4) extended to the end of the beam has not been studied. It is noteworthy that the theoretical analysis methods used in the design of IT deep beams, which shall be discussed later, also didn't account for the effect of the hanger reinforcement and ledge length.

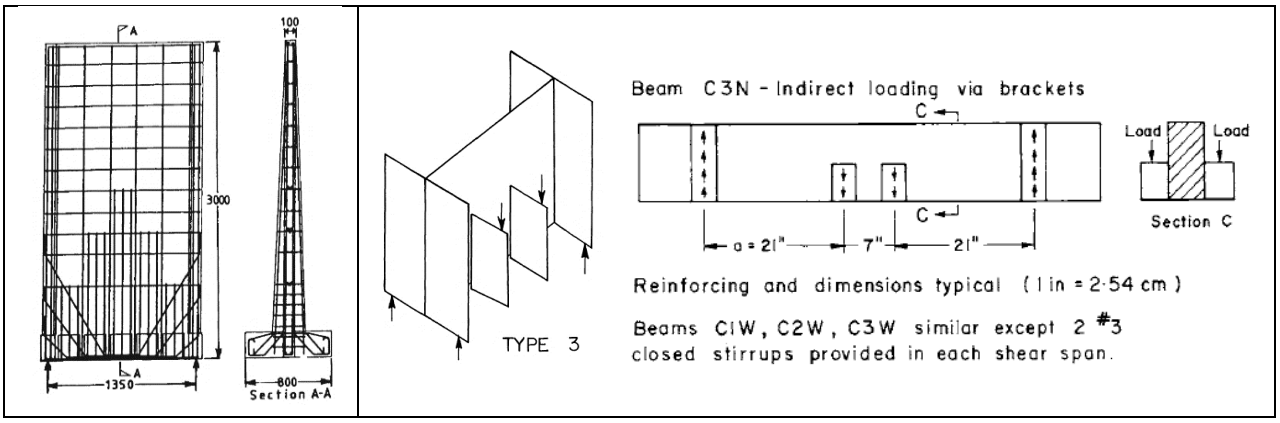

(a) Hanger reinforcement up to the mid height of IT deep beam [4]

(b) Unrealistic supporting conditions [10, 11]

Figure 4. Examples from the literature of some of the tested specimens

1.2. Research Significance

Based on the above, an experimental program was needed to investigate the different reinforcement parameters of the IT deep beams. It is important to understand the effect of changing the diameter and ratio of the hanger reinforcement on the capacity of the IT deep beams. The hanger reinforcement arrangement needed to be examined to check the effect of changing the reinforcement spacing and determine the maximum spacing required to ensure the transmission of the tension force from the ledge to the web. Moreover, the impact of placing hanger reinforcement within a distance less than that calculated according to the 45-degree concept of load spreading and the minimum hanger reinforcement ratio required to be placed within the load plate length to guarantee that the hanger has sufficient capacity to achieve complete load transmission need to be studied.

An experimental program was conducted to investigate the effect of the aforementioned parameters on the behavior and capacity of IT deep beams by testing eight specimens of different reinforcement parameters. The ledge of all specimens was of type (4) and extended to the end of the beams, which allowed the specimens to sustain extra loads when compared to beams with short ledges and simulate the most common shape in structural members. The effect of the long ledge will be studied briefly later in this paper and extensively through a parametric study in the following publication.

Unlike most research, the vertical and horizontal web reinforcements were tested separately to determine the influence of each parameter on the beam capacity. A FE numerical model using ABAQUS [20] software was developed to predict the behavior of IT deep beams considering material nonlinearity. The parameters proposed in the literature were modified, and the output of the FEM was compared and validated using the experimental program results. The results showed good agreement with the experimental results.

A comparison between the literature review results and the results obtained from the experimental and FE models will be presented within this research. Noting that the performed analysis related to the hanger reinforcement diameter, arrangement, ratio, and beams with type 4 ledge has not been studied in past research, and not sufficient data is available in the literature regarding this topic.

Figure 5 shows a flowchart for the process of the methodology followed in this study.

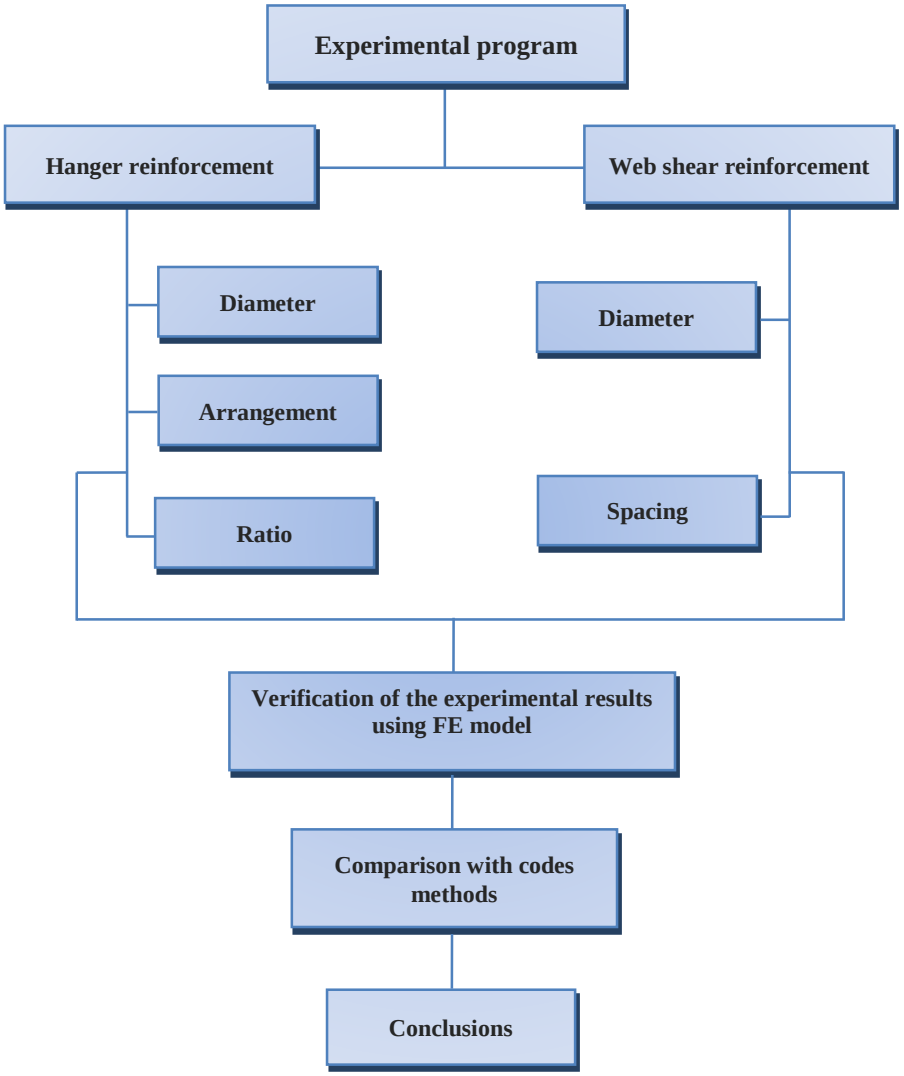

Figure 5. Flowchart of the work methodology

2. Experimental Program

To accomplish the objectives of this study, an experimental program was established to investigate the influence of hanger and web shear reinforcement on the behavior of inverted-T deep beams, as very little relevant information was available, as mentioned earlier in the literature review. The experimental program comprised eight specimens divided into six groups. The objective of the test was to examine the influence of the following parameters on the capacity and behavior of the IT deep beam:

- Hanger reinforcement diameter;
- Hanger reinforcement arrangement;
- Hanger reinforcement ratio;
- Vertical web reinforcement ratio (spacing and diameter);
- Horizontal web reinforcement spacing.

2.1. Specimen Details

The dimensions of the specimens in this research were selected based on calculations performed according to the strut and tie model (STM) provisions, which were adopted by many structural codes, including ACI 318-19 [2] and ECP-203 [1]. The width of the hanger ties adopted by the STM method is based on a 45-degree spread of the load on the ledge under the loading plates [12]. Vertical hanger bars were positioned at the loading point, with the tie corresponding to the bearing pad center. Figure 6 shows the load transfer in the STM for the web and ledge of the IT deep beam.

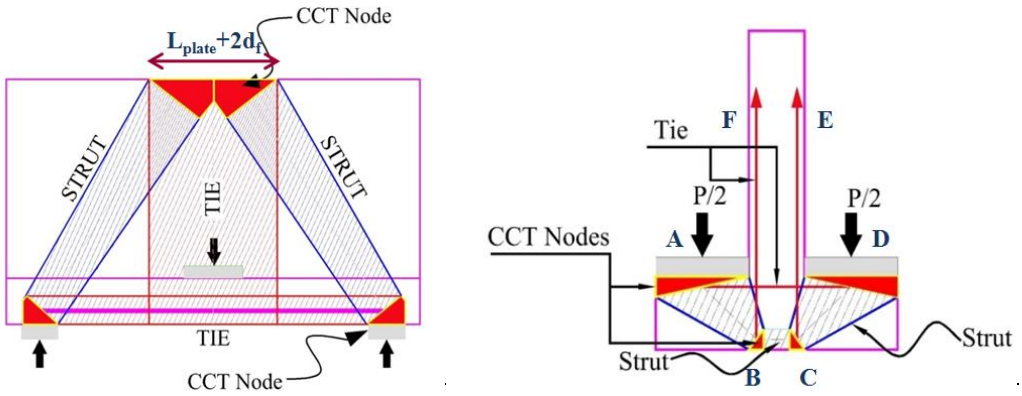

(a) Web STM (b) Ledge STM

Figure 6. Load transfer in strut and tie model

The strut-node interfaces of the diagonal strut were designed to govern the failure. The dimensions of the web and ledge were also checked by using the empirical method of the AASHTO LRFD Bridge Design Specifications-2020 [17]. The AASHTO LRFD method is based on preventing the five potential types of failure in the web and ledge: shear friction, punching shear, failure of the hanger reinforcement, flexural failure of the ledge reinforcement, and bearing failure of concrete under the loading point.

Dimensions and reinforcement details of the control specimen are shown in Figure 7. The concrete dimensions were kept constant for all specimens. The total beam length was 1400 mm, while the distance between support plates was 1200 mm. The web width was 120 mm, the beam depth was 800 mm, and the ledge depth was 150 mm. The loading plate size was 200×200 mm, while the support plates were 100×300 mm. The flexural reinforcement ratio was about 0.5%, as obtained from the strut and tie model. Ledge reinforcement was constant in all specimens of diameter T12 and spacing, as shown in Figure 7. Hanger and web shear reinforcement (vertical and horizontal) are varied as shown in Table 1, Figures 8, and 9.

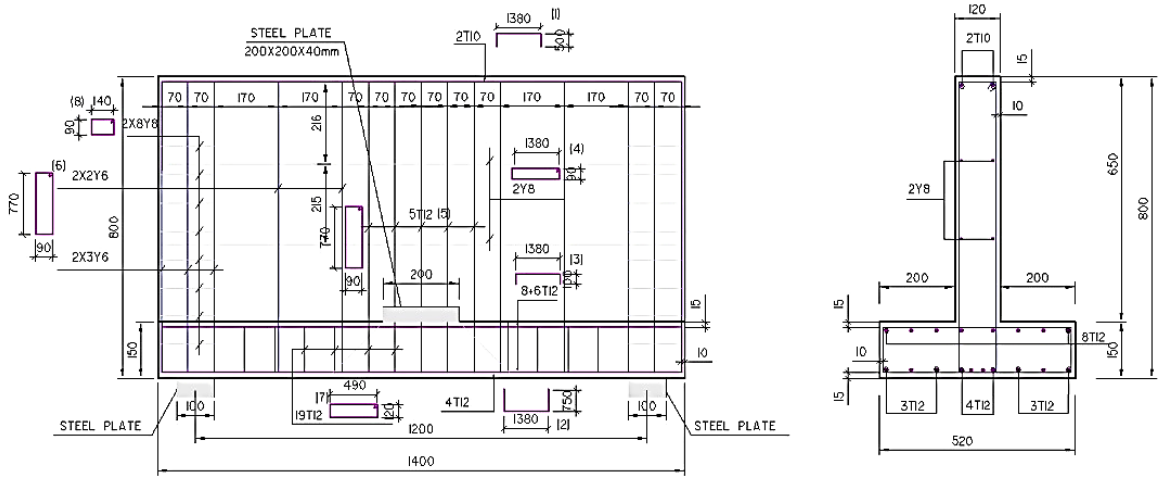

Figure 7. The dimensions and reinforcement details of the control specimen

Table 1. Summary of beam details

Specimen No.	Hanger RFT.		VL. RFT.		HL. RFT.		fcu (MPa)
	Rft.	%Rft.	Rft.	%Rft.	Rft.	%Rft.	
IDB1	5T12+2Y6	2.25	Y6@170mm	0.28	Y8@220mm	0.39	28.4
IDB2	3T16	2.20	Y6@170mm	0.28	Y8@220mm	0.39	26.9
IDB3	7T10	2.00	Y6@170mm	0.28	Y8@220mm	0.39	33.4
IDB4	7T16	5.10	Y6@170mm	0.28	Y8@220mm	0.39	28.8
IDB5	3T16	2.20	Y6@170mm	0.28	Y8@220mm	0.39	28.8
IDB6	5T12+2Y6	2.25	Y6@85mm	0.56	Y8@220mm	0.39	35.7
IDB7	5T12+2Y6	2.25	Y10@170mm	0.77	Y8@220mm	0.39	35.7
IDB8	5T12+2Y6	2.25	Y6@170mm	0.28	Y8@110mm	0.78	33.4

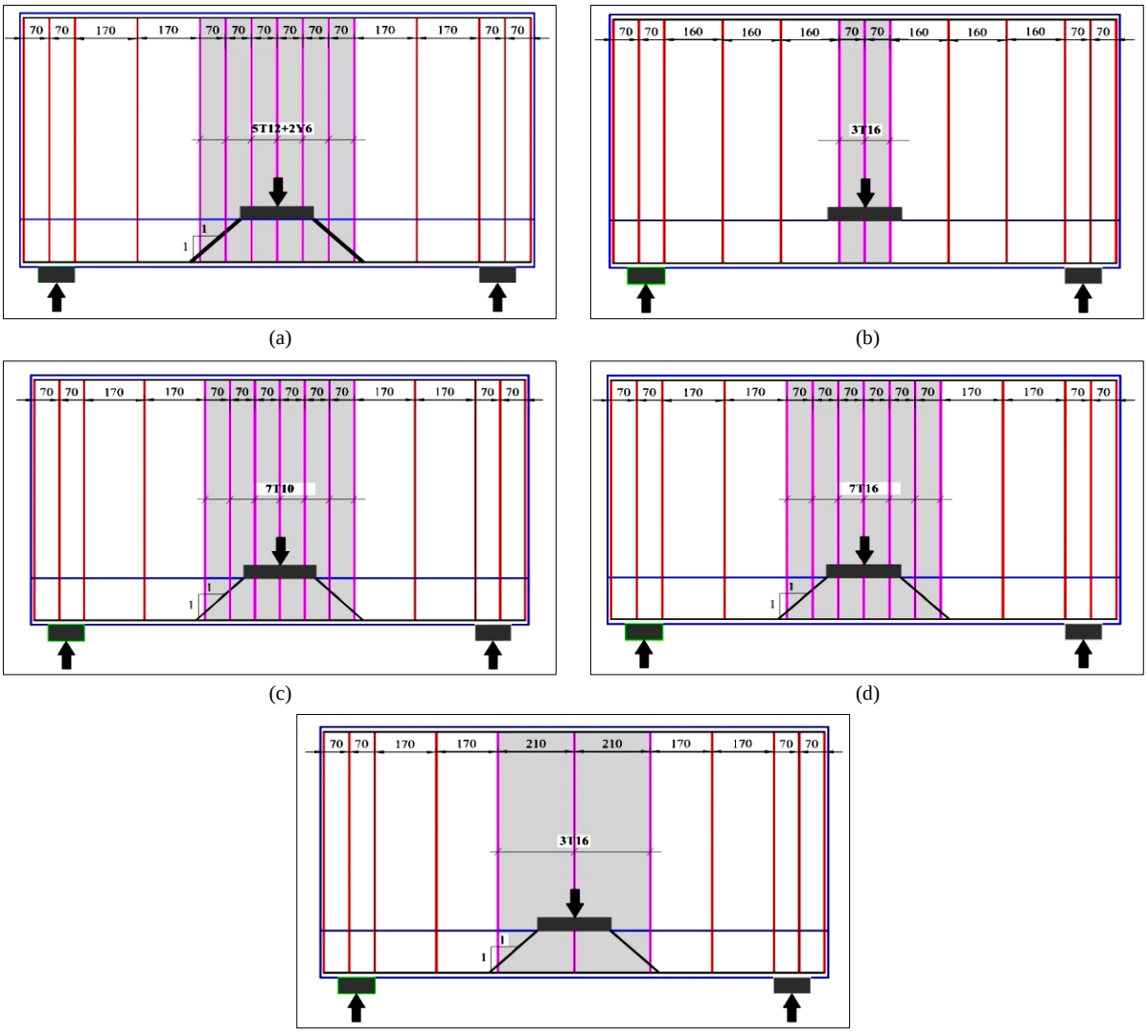

Figure 8. Reinforcement details for specimens with variable hanger reinforcement

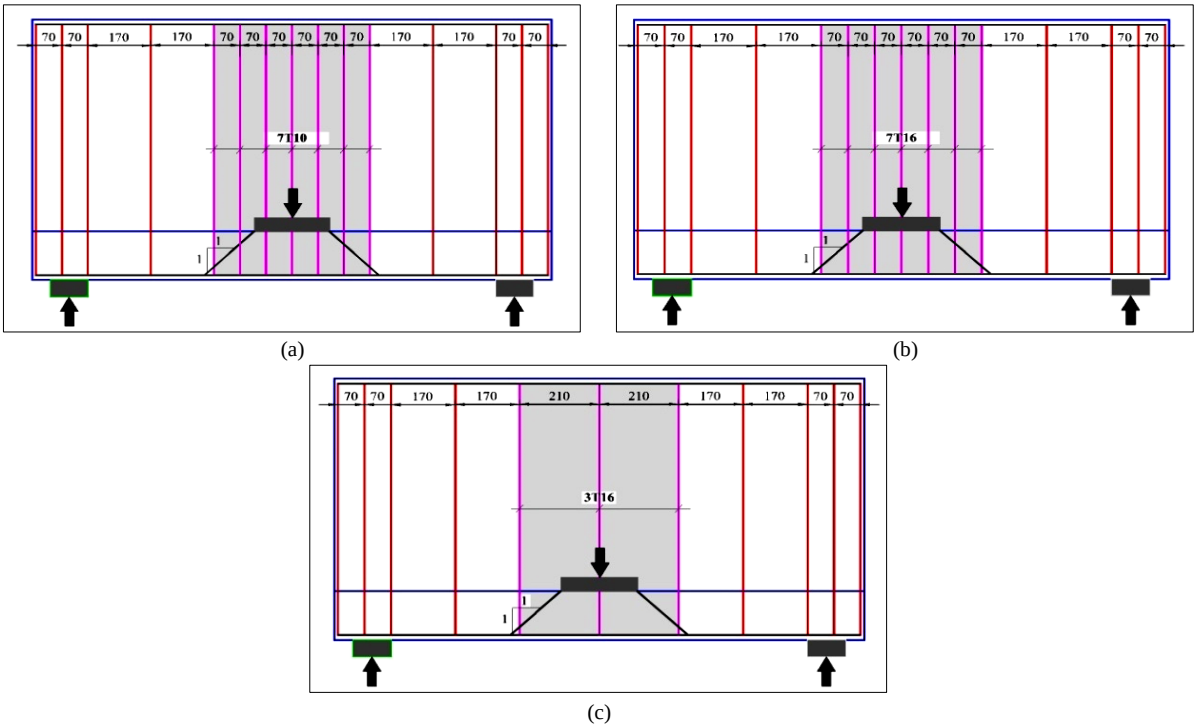

Figure 9. Reinforcement details for specimens with variable web shear reinforcement

Preliminary calculations were performed before the test by using design codes [1, 2, 14] and theoretical methods. The strut and tie models and the ABAQUS [20] program were used to estimate the expected capacity of the tested specimens and the required hanger, longitudinal, ledge, and web shear reinforcement. As no specific recommendations are included in the codes regarding the maximum ratio of the hanger reinforcement, the diameters and spacing were specified to meet both the capacity requirements and to facilitate the execution and concrete pouring of the specimens.

The experimental variables shall be as follows:

Hanger reinforcement diameter: To evaluate the influence of changing hanger reinforcement diameter two specimens ID1 and IDB3 of different hanger diameters with almost the same reinforcement ratio ranging from 2% to 2.25% were compared.

Hanger reinforcement arrangement: In this group, three specimens (IDB 1, 2 & 5) of different arrangements of hanger reinforcement (spacing and distribution length) were evaluated, keeping almost the same reinforcement ratio of about 2.2%.

Hanger reinforcement ratio: The effect of increasing the hanger reinforcement ratio from 2.0% to 5.1% was investigated by comparing the results of three specimens (IDB 1, 3 & 4).

Vertical and Horizontal Web Reinforcement ratio: The impact of increasing vertical web shear reinforcement in IDB1, ID6, and IDB7 from 0.28% to 0.55% and 0.77% was captured by testing specimens of different spacings and diameters. While two specimens, IDB1 and IDB8, with different horizontal reinforcement ratios of 0.39% and 0.78% were tested. These ratios were specified to be more than the minimum reinforcement ratio for deep beams (0.25% in each perpendicular direction) as recommended in ACI 318-19 [2] to effectively restrict the distribution of the diagonal cracks under service loads, the diagonal crack width, and allow for sufficient redistribution of forces to achieve full strength of compression struts.

The variables were divided into 6 groups, Groups 1,2, and 3 for studying hanger reinforcement, and groups 4,5, and 6 are related to studying web shear reinforcement as shown in Table 2.

Table 2. Specimens' groups

Group (1)	Group (2)	Group (3)	Group (4)	Group (5)	Group (6)
Hanger Reinforcement			**Web Shear Reinforcement**		
Hanger Reinforcement Diameter	Hanger Reinforcement Arrangement	Hanger Reinforcement Ratio	Vertical Web Reinforcement Spacing	Vertical Web Reinforcement Diameter	Horizontal Web Reinforcement Spacing
IDB 1& 3	IDB 1, 2& 5	IDB 1, 3 & 4	IDB 1 & 6	IDB 1 & 7	IDB 1 & 8

Figures 8 and 9 show the reinforcement details of the tested specimens.

2.2. Materials

The specimens were constructed using conventional materials and methods. The concrete mixture was designed to reach the target cube concrete compressive strength of 28.5 MPa. The mixture components were 290 kg of ordinary Portland cement type I, 1160 kg of natural crash well-graded stone as coarse aggregate (gravel) with a maximum size of about 13 mm, 650 kg of sand with a 2.36 mm maximum size as fine aggregate according to ASTM standard [22, 23], 300 kg of water, and 3 kg/m3 BVF.

Beams were tested approximately 28 days after concrete placement. Steel reinforcement was tested in the material laboratory of the Faculty of Engineering at Cairo University, satisfying the requirements of the Egyptian code and specifications to obtain the actual tensile stress. The yield stress of steel reinforcement was 382 MPa for Y6 and Y8, 578 MPa for T10, 515 MPa for T12, and 553 MPa for T16. Reinforcement details of the specimens and the cube compressive strength of concrete after 28 days (f_{cu}) are provided in Table 2. From Table 1, it can be noted that higher values of concrete compressive strength were observed in specimens IDB3, IDB6, IDB7, and IDB8 when compared with other specimens. This increase is because the cement used in these specimens was imported from another supplier. The average value of concrete compressive strength of all specimens was 31.39 MPa, and the coefficient of variation was 11.3%, which are considered acceptable values.

2.3. Testing Procedure

The specimens were tested at the Concrete Research Laboratory at the Faculty of Engineering-Cairo University. The load was applied via a 5000-kN hydraulic loading machine, as shown in Figure 10. A 1200-kN loading cell attached to an 8-channel data logger was used to transmit the load from the machine to the specimens. The loading cell was placed on top of a U-shaped steel frame. The steel frame was designed to sustain a concentrated load of up to 1200 kN. The U-

shaped steel frame was designed and manufactured specifically for this loading setup. It consists of IPE beam no. 300 with two plates welded to the web at each side of 6 mm thickness. The beam was stiffened with three stiffeners of 6mm thickness on each side. The beam was fixed to two solid square section steel columns 150×150 mm using 20 mm thick plates by 4 bolts M12. The base of the columns was welded to two plates 200×200×40 mm. The U-shaped frames shown in Figures 10a and 10b were evenly placed on the ledges on both sides of the web.

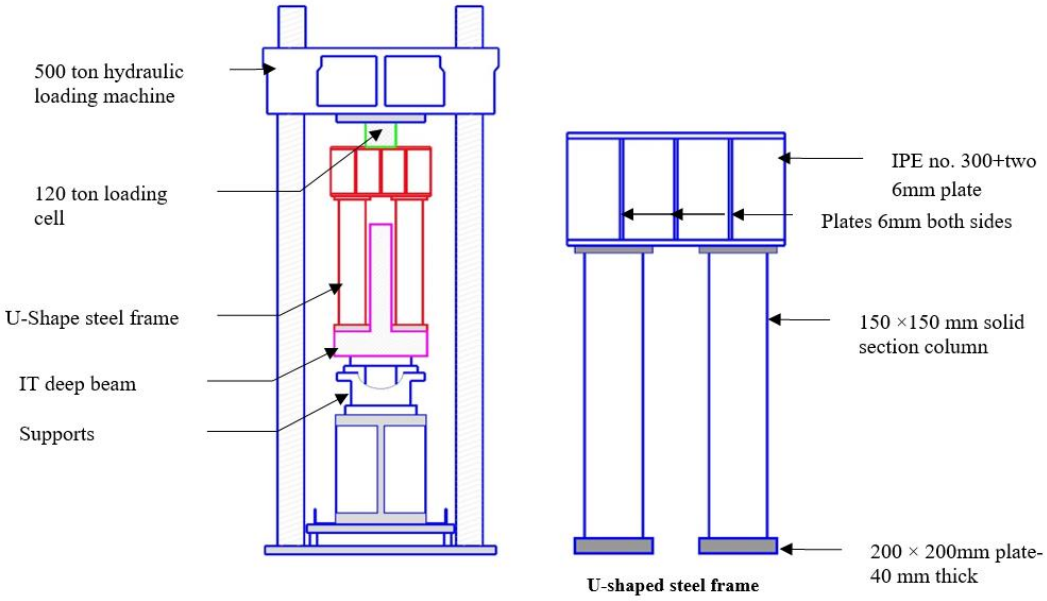

(a)

(b)

Figure 10. Test setup: (a) Schematic, (b) photos

Two linear voltage displacement transducers (LVDTs) at the mid-span under the beam web and the ledge were used to capture the vertical deflections. Figure 10 shows the loading and support points. Test specimens were monotonically loaded (10 kN) with an increment every 30 seconds until failure. After each load increment, cracks were marked.

Several electrical resistance strain gauges (ERSs) were used to measure the local strains in the longitudinal and shear reinforcement, while the strain in the concrete along the diagonal compression area was measured by other ERSs connected to the concrete surface. Figure 11 shows the arrangement of the strain gauges and LVDTs. A static data acquisition system was used to measure and electronically store the applied load, vertical displacements, and strain readings during the test at each load increment.

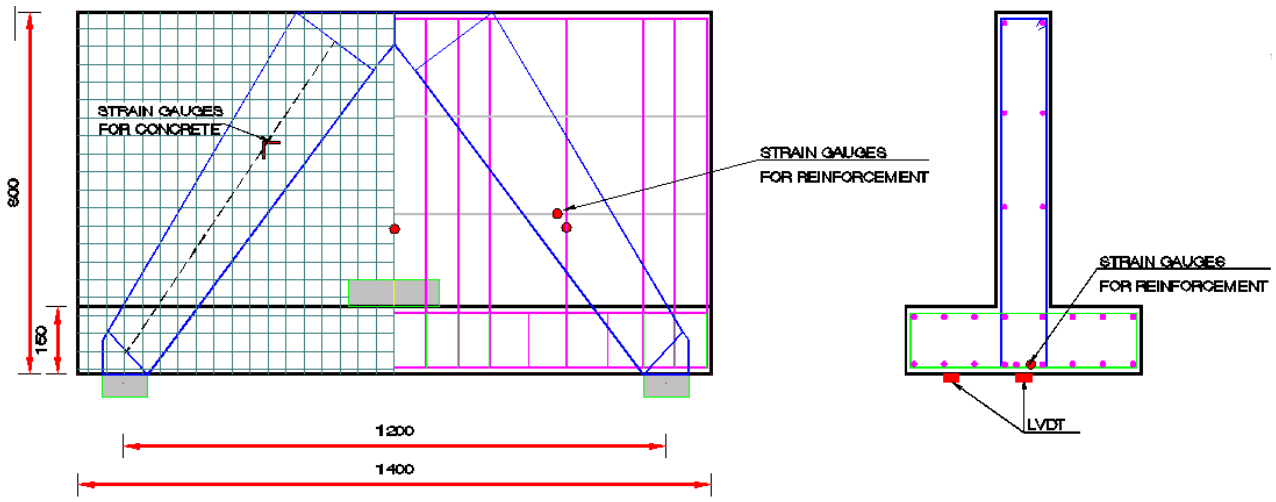

Figure 11. Locations of ERSs in tested specimens

3. Test Results

3.1. Crack Propagation and Modes of Failure

Figure 12 illustrates the crack patterns of the eight specimens at failure. The figures also show the loads at which each crack was first detected and the crack extension at that load. At the initial loading stage, all specimens behaved elastically, and no visible cracks were observed on the surface of the concrete. The first diagonal crack was usually formed at approximately 30 to 40% of the ultimate strength at the web surface near the middle of the shear span in the direction of the load support, and then the cracks propagated upward to the compression zone and downward to the ledge. It can be seen from the figures that IDB1, IDB3, IDB6, IDB7, and IDB8 have almost the same first cracking load. This behavior until the appearance of the first crack can be explained by the fact that these specimens have almost the same hanger reinforcement ratio and arrangement; on the other hand, IDB4 and IDB5 had the highest and least cracking loads, respectively.

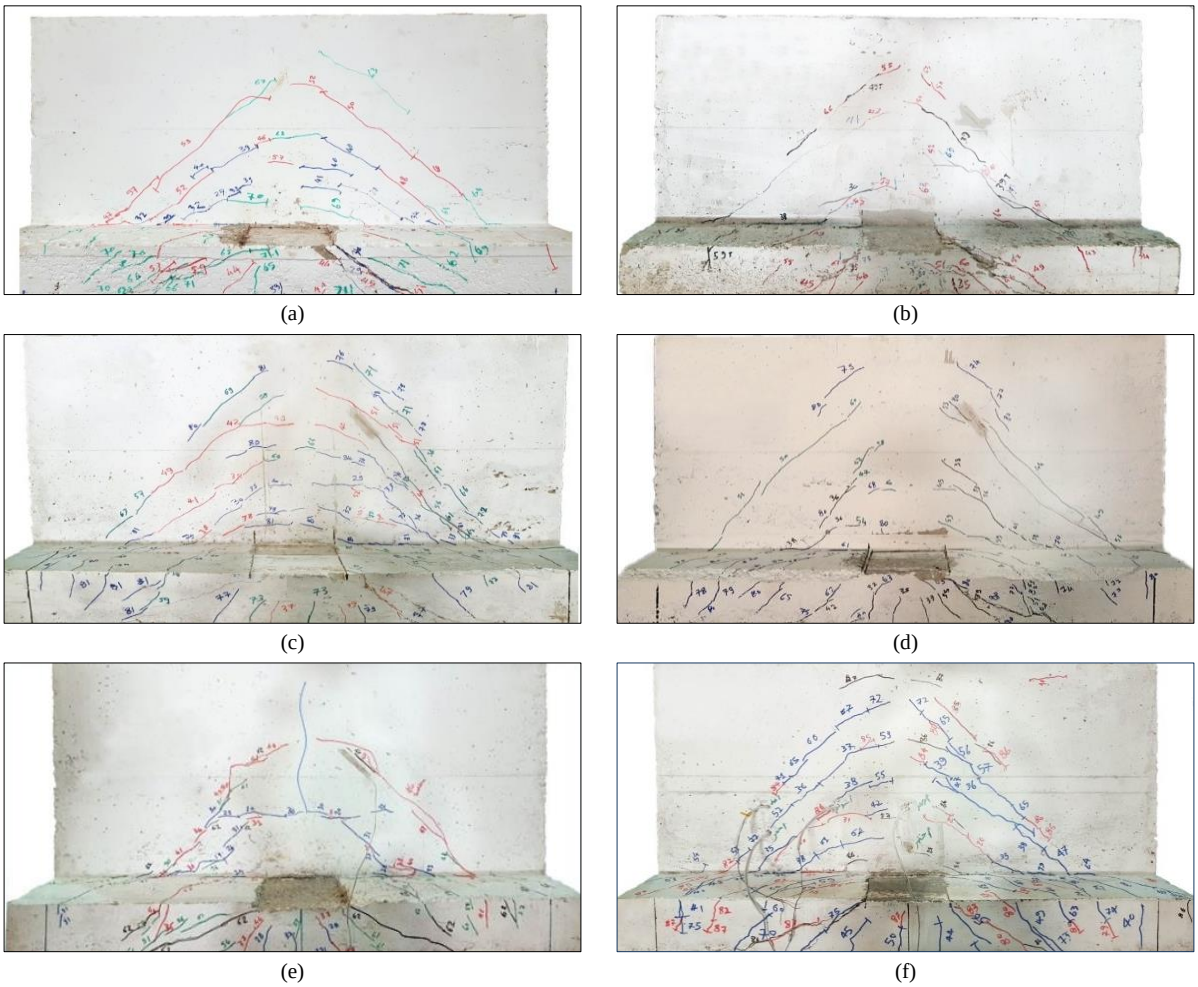

(a) (b)

(c) (d)

(e) (f)

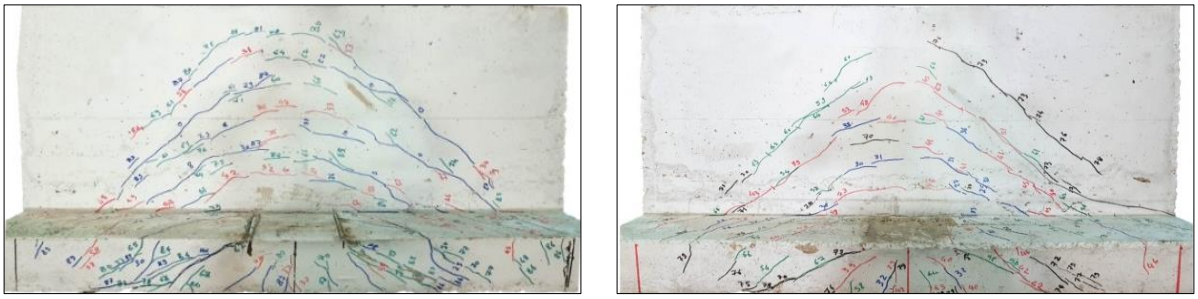

(g) (h)

Figure 12. Crack patterns

Flexural cracks initially started at the bottom in the midspan region of the beam. On further loading, the number of flexural cracks increased gradually. As the loading increased, some of the new parallel diagonal cracks were formed and rapidly expanded in width and length, while the existing flexural cracks in the pure bending zone spread slowly and stabilized. These flexural cracks indicate that the long ledge extending to the supports contributes with the web to transferring the load to the supports, which increases the capacity of the IT deep beam.

Thereafter, all specimens went through a short stored-energy phase, and the previously occurring diagonal cracks nearly stopped widening and extending. All cracks are distributed symmetrically about the specimen centerline, confirming the occurrence of a direct strut transfer mechanism. Finally, six specimens failed in combined shear-flexure-punching under the loading plate except for IDB4 and IDB5, where IDB4 failed in combined shear-punching under the loading plate and IDB5 failed in combined flexure-punching under the loading plate. For IDB5, the insufficient number of hanger reinforcements passing through the loading plate region led to the formation of a vertical crack at the middle of the web, causing the beam to act as a slender beam rather than a deep beam. This behavior caused a significant reduction in the beam capacity, as will be presented later. A noticeable spread of cracks in the specimens containing a large amount of vertical web shear reinforcement (IDB6 and IDB7) was observed; furthermore, the propagation of cracks along the beam height for these specimens was the highest among all specimens. IDB5 has the least crack propagation as the effectiveness of the arch action tends to decrease. The large spacing between the hanger reinforcements made the hanger unable to transfer the load to the top of the beam, which caused the flexural behavior to become more dominant. For IDB4, the cracks were definite and concentrated on both sides of the loading plates without intersecting the middle region.

3.2. Load-Deflection Curves

As a result of the change in the compressive strength of the concrete of the tested specimens, as indicated in Table 2, it was necessary to eliminate the effect of this parameter on the results. As the specimens encountered sectional shear failure as the diagonal tension in the web affected the shear capacity, the ultimate load was normalized with respect to $\sqrt{(f_{cu}/28.5)}$ to consider the unavoidable differences in the actual compression strength of concrete. This term was specified for normalization as the specimens experienced shear failures. Therefore, normalizing the results by $\sqrt{(f_{cu})}$ was appropriate, and then it was multiplied by $\sqrt{28.5}$ which is the value of the cubic strength of the concrete mix, to obtain the specimens' failure load, which is not affected by the change in concrete strength of the tested specimens. Table 3 and Figure 13 display the capacity and mode of failure of the eight specimens.

Table 3. Cracking and ultimate loads of the specimens

Specimen no.	P_{crack} (kN)	P_u (kN)	Modes of failure
IDB1	264.9	729.9	Combined Shear-Flexure-Punching
IDB2	294.3	750.5	Combined Shear-Flexure-Punching
IDB3	264.9	761.3	Combined Shear-Flexure-Punching
IDB4	323.7	796.6	Combined Shear-Punching
IDB5	196.2	612.2	Combined Flexure-Punching
IDB6	255.1	814.3	Combined Shear-Flexure-Punching
IDB7	264.9	825.1	Combined Shear-Flexure-Punching
IDB8	264.9	738.8	Combined Shear-Flexure-Punching

P_{crack}: First crack load, P_u: Failure load

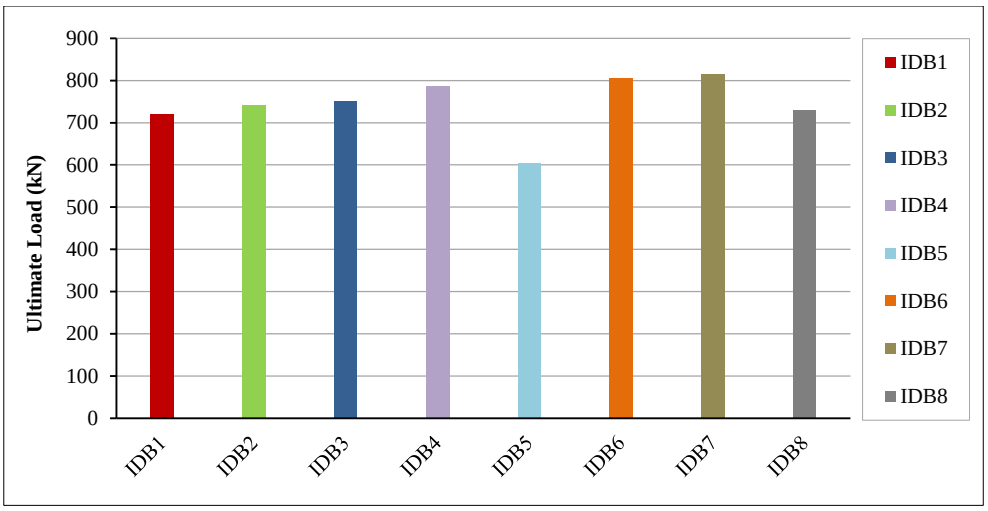

Figure 13. Ultimate capacity of tested IT deep beams

The deflection behavior at mid-span was measured using LVDTs under the beam web and ledge. The deflection was recorded with load increments up until specimen failure. Figure 14 presents the load-mid-span deflection record of the eight specimens. It can be seen from the figure that during the initial loading phase, there was a linear relationship between the applied load and the specimens' mid-span deflection. The formation of critical shear cracks is evidenced in the curves by a sharp increase in deflection or a sudden decrease in applied load. After reaching the ultimate shear and flexural capacity, a short straight segment was noticed in the curves, and then the applied load to the beams decreased rapidly.

As mentioned before, the hanger is responsible for transmitting the loads applied to the ledge to the upper parts of the web of the IT beam. Group (1) showed that changing the hanger reinforcement bar diameter while keeping almost the same area of reinforcement and the same spacing between the hanger's bars has an insignificant effect on the beam capacity, as shown in Figure 14a. This behavior shows that if the required reinforcement ratio and the proper spacing are fulfilled in the hanger reinforcement, the hanger will be able to transmit the load to the web regardless of the hanger diameter.

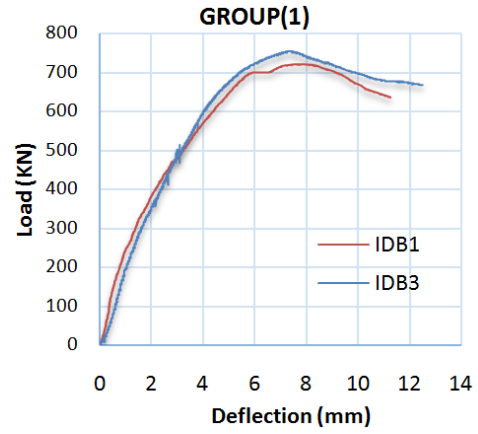

(a) Effect of hanger reinforcement diameter

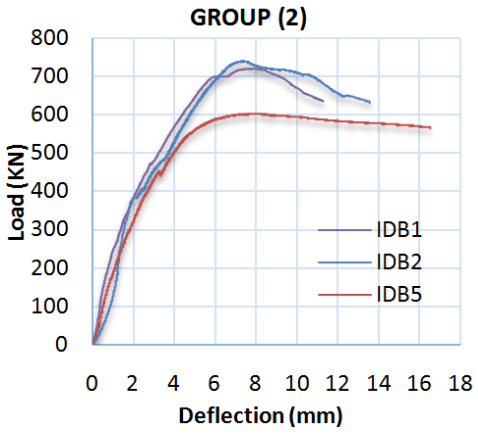

(b) Effect of hanger reinforcement arrangement

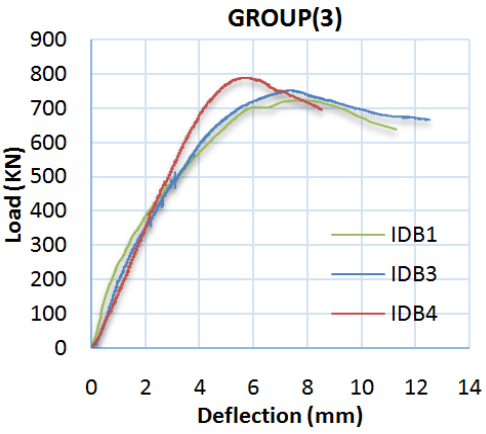

(c) Effect of hanger reinforcement Ratio

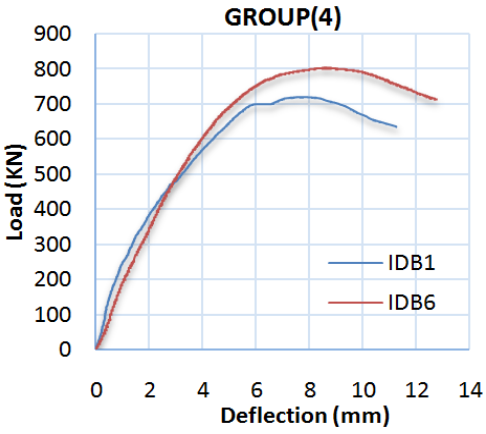

(d) Effect of vertical Web Reinforcement Spacing

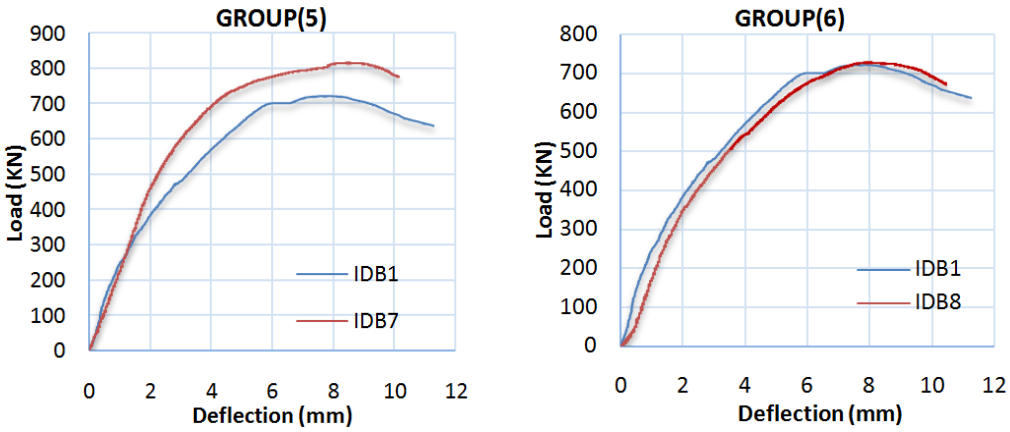

(e) Effect of vertical Web Reinforcement Diameter (f) Effect of horizontal Web Reinforcement Diameter

Figure 14. Load-deflection curves

Figure 14b shows that the stiffness of all specimens in Group (2) was similar up to the maximum load. Whereas, IDB5 with the larger spacing between hanger reinforcements had a post-peak ductility, indicating a flexure behavior of the beam. The beam capacity has also decreased by about 20%. This behavior indicates that the hanger spacing of IDB5 exceeded the maximum required spacing necessary to enable the hanger to transfer the full load to the web. Hence, the arch action was not complete, and the flexural behavior became more dominant. Also, the non-homogeneity of IDB1 caused by using two different bar diameters for hanger reinforcement caused a slight reduction in beam capacity. Also, it should be noticed that concentrating the hanger reinforcement only at the loading plate distance in IDB2, where the 45-degree concept of load spreading was not applied as proposed in the literature review, did not affect the capacity of the IT deep beam. This output indicates that as long as the required hanger reinforcement ratio is achieved, even if it is concentrated at a distance less than (W+2df), the beam will be able to sustain the same ultimate capacity.

Comparing the results of Group (3) where the hanger reinforcement ratio was increased from 2.0% to 5.1%, more than twice the original value, the curve in Figure 14c showed that beam IDB4 had a stiffer load-displacement response after reaching the first diagonal crack. The mid-span deflection of IDB4 at failure decreased by about 15.5% and the ultimate load increased by 6.5%, indicating that the increase in the hanger reinforcement ratio enabled the hanger to transfer the full load to the top of the beam and utilized the arch action mechanism. The curve also shows a more brittle behavior of IDB4 than IDB1 and IDB3.

A diagonal crack tends to form when the concrete diagonal tension resistance is less than that required to resist the loads applied to the beam. Beam web reinforcement is essential to transfer the induced shear forces across diagonal cracks. For top-loaded deep beams, the load helps the concrete resist diagonal tension stresses resulting from the shear on the beam. For IT-deep beams where the forces are hung from the bottom, vertical tension stresses are reformed in the beam above the loading point. The vertical tension stresses tend to increase the probability of concrete diagonal tension cracking. IT beams are thus subjected to diagonal tension cracking at lower load levels than top-loaded deep beams. Increasing the vertical web reinforcement ratio either by reducing bar spacing or increasing diameter will lead to a significant increase in both the mid-span deflection and applied load, as shown in Groups (4 and 5). By comparing the curves in Figures 14d and 14e of Groups (4) and (5), it can be deduced that decreasing vertical web shear reinforcement spacing is more beneficial than increasing bar diameter. The significant effect of the vertical shear reinforcement may be attributed to the fact that it increases the compression capacity of the strut, reduces the crack width, and also allows excess shear reinforcement to be used as a hanger reinforcement [15]. The behavior of Group (6) shown in Figure 14f shows that increasing the horizontal web reinforcement diameter increased the beam strength by an insignificant ratio of 1.27%. In previous research on reinforced concrete deep beams [15, 16], beams with horizontal reinforcement of 0.3% showed slightly higher shear strength than those with a ratio of 0.6%. This result contradicts the output of this research and also other research performed on deep beams by Birrcher et al. [24], which found that horizontal web shear reinforcement has little effect on increasing the shear strength.

3.3. Strain in Reinforcement

Figure 15 illustrates the variation of the reinforcement strain of the eight specimens of IT deep beams versus the total applied load. Figure 11 shows the location of strain gauges and LVDTs in the tested specimens. A minimum of four strain gauges were used in each specimen. One strain gauge was located on the middle hanger. One gauge was placed on the midpoint of the longitudinal reinforcement. The strain in the web shear reinforcement was measured using two gauges placed on the vertical and horizontal stirrups. While in IDB8, where the effect of increasing the ratio of horizontal web reinforcement was under study by reducing the spacing between horizontal stirrups, two gauges were located on the horizontal stirrups. The strain gauges of IDB6 and IDB7 didn't work properly during the test, so their results were excluded from the results presented in Figure 15. The strain in the reinforcement of these specimens will be investigated using the finite element model later.

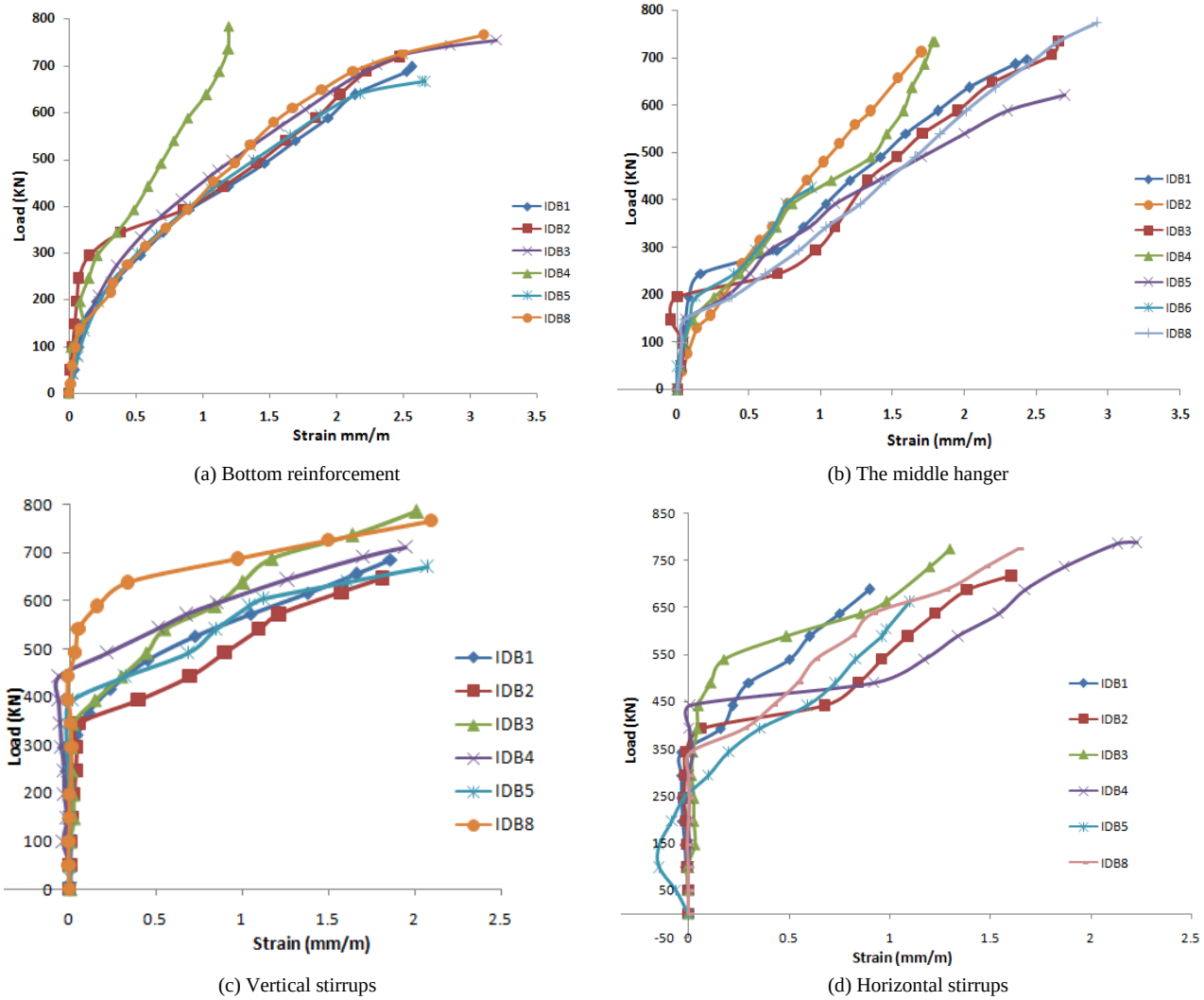

(a) Bottom reinforcement

(b) The middle hanger

(c) Vertical stirrups

(d) Horizontal stirrups

Figure 15. Load- Strain curves in tested specimens

3.3.1. Bottom Reinforcement

All the tested specimens reached the yield point at maximum load except IDB4. The results explain that flexure failure occurred in all specimens except IDB4. The effect of the long ledge extending to the supports increased the probability of the flexural behavior of the specimens. The increase in the hanger reinforcement ratio in IDB4 decreased the mid-span deflection significantly, which caused an increase in the flexural stiffness of the IT deep beam, which prevented the occurrence of flexure failure.

3.3.2. Hanger Reinforcement

The ERS of the middle hanger of all specimens reached yield stress at maximum load except the middle hanger of IDB2 and IDB4, which reached only 64% and 68% of the yield stress at maximum load, respectively. From the strain results, it can be concluded that concentrating the hangers in the plate region as in IDB2 or increasing the hanger reinforcement ratio as in IDB4 decreases the strain in the mid-hanger, which indicates that the hanger reinforcement in these two specimens exceeded the reinforcement needed to transfer the load to the top of the beam.

3.3.3. Vertical and Horizontal Web Reinforcement

As seen in Figures 15c and 15d, before the formation of the first diagonal crack, the strain of the web reinforcement was almost zero as the shear force was carried by the concrete without any contribution from the web shear reinforcement. After the formation of the first diagonal crack, the stresses started transmitting to both vertical and horizontal web shear reinforcements, causing a sudden increase in their strains. As the load was increased, the vertical stirrups of all specimens yielded, while only the horizontal web reinforcement of IDB4 achieved the yield point. The yield of the horizontal stirrups of specimen IDB4 occurred because the load in IDB4 was transmitted completely to the supports by the arch action along the diagonal strut without any contribution from the beam action that occurred in all other specimens.

4. Finite Element Modeling (FEM)

The finite element program ABAQUS [20] was used to study the behavior of reinforced concrete IT-deep beams. The FE model was validated using the experimental analysis results. The values of concrete compressive strength and steel reinforcement yield strength were explained previously in the material clause. These values were used as input in the finite element program. An extensive parametric study will be included in the following publication. This study shall comprise the effect of the span-to-depth ratio to capture the behavior of the IT deep beam and obtain L/d values at which the IT beam behavior changes from deep to slender beam. Moreover, the effect of ledge dimensions (length, depth, and width), longitudinal reinforcement, and ledge reinforcement shall be studied.

4.1. Concrete

The concrete damage plasticity (CDP) in ABAQUS [20] can be used for defining the material properties of concrete in IT-deep beams. The CDP model assumes that tensile cracking and compressive crushing are the two principal failure mechanisms in concrete. The yield surface evolution is determined by two hardening variables, tension and compression equivalent plastic strains, respectively. Each is associated with degradation mechanisms under tensile or compressive stress conditions, as indicated in Figure 16.

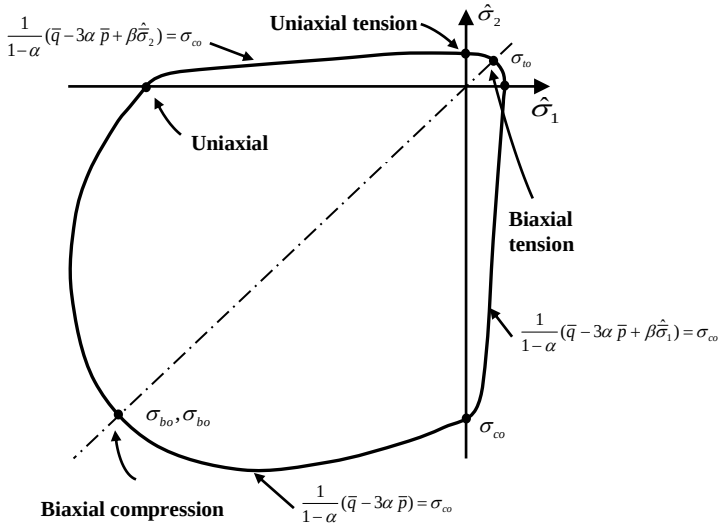

Figure 16. Yield surface in plane stress

In this study, the stress-strain models for concrete in compression and tension included in the CEB-fip model code [25] were used in ABAQUS [20]. The post-cracking tension softening behavior is defined by using a linear post-peak tension softening model as tensile stress versus crack width behavior. Under uniaxial compression, the behavior is linear until the initial yield, f_{co}. In the plastic regime, the response is typically characterized by stress hardening followed by strain softening beyond the maximum stress, f_c, as shown in Figure 17. This representation, though somewhat simplified, captures the main characteristics of the concrete response.

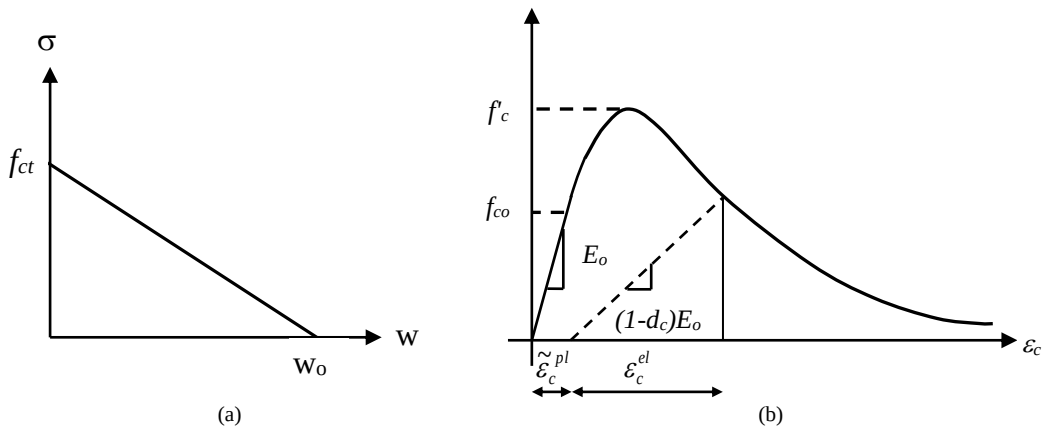

Figure 17. Concrete response due to (a) Uniaxial tension, (b) Uniaxial compression

4.2. Steel

As described in ABAQUS/CAE 2017 [20], the constitutive behavior of steel reinforcement can be predicted using an elastic-perfectly plastic model. In this approach, the steel reinforcement behavior is elastic up to the yield stress. After that, the reinforcement yields under constant load, as shown in Figure 18. The interaction between the concrete and steel reinforcement is modeled, assuming that the steel is embedded in the concrete with a perfect bond.

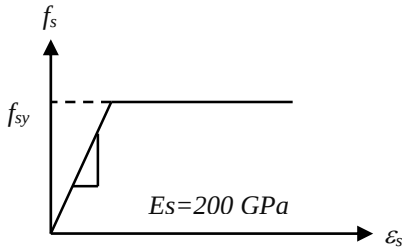

Figure 18. Stress-strain relationship of steel reinforcement

A three-dimensional finite element model (FEM) was used for the numerical analysis of the experimentally tested reinforced concrete IT deep beams. A 3D-8-node deformable element linear brick, C3D8R, was used for the modeling of the concrete and steel plates under applied load and at supports. Longitudinal, horizontal, and vertical reinforcement in reinforced concrete beams is modeled by using a wire-element 2-node linear 3-D truss T3D2 embedded in the concrete element to simulate a perfect bond. The use of the embedded model allows an independent choice of the mesh size of concrete. The mesh size used was 25mm. The interaction between both load and support plates and the concrete beam was modeled as a tie constraint. The load was applied on two loading plates positioned above the ledge of the IT deep beams, while the supports at both ends were modeled as hinged rollers by preventing translation in all directions at one end and allowing only translation along the beam length of the other end to simulate the boundary conditions of the tested specimens. The parameters of the CDP model are listed in Table 4, and the details of the FEM used in the validation are represented in Figure 19.

Table 4. CDP model's input parameters

Definition	Notation	Selected Value
Dilation angle	Ψ	38
Tensile to compressive meridian ratio	Kc	0.667
The ratio between biaxial state strength to uniaxial state strength	$\sigma_{\beta 0}/\sigma_{X0}$	1.16
Eccentricity	ε	0.10
Viscosity parameter	μ	0.0001

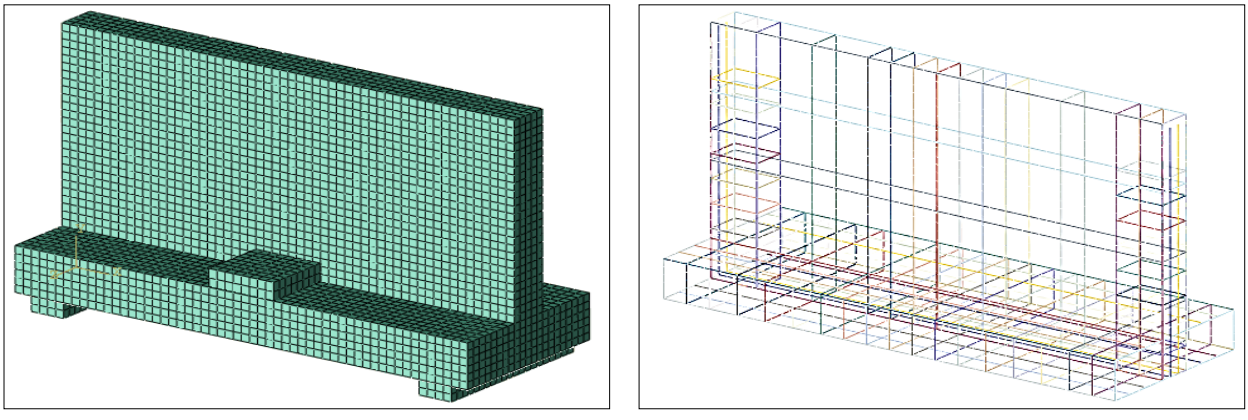

(a) Used Mesh in the Validation (b) Steel Reinforcement

Figure 19. FE Model Details

Before studying the beams tested in the experimental program, the ABAQUS FE model was first verified by analyzing one of the specimens tested by Varney et al. (2013) [16]. Figure 20 shows the concrete dimensions and the reinforcement details of the chosen specimen beam DL1-42-2.50-03. This step was essential for both validating the FE model and predicting the expected ultimate load of the specimens and the capacity of the machine that will be used during the test before proceeding with the experimental program.

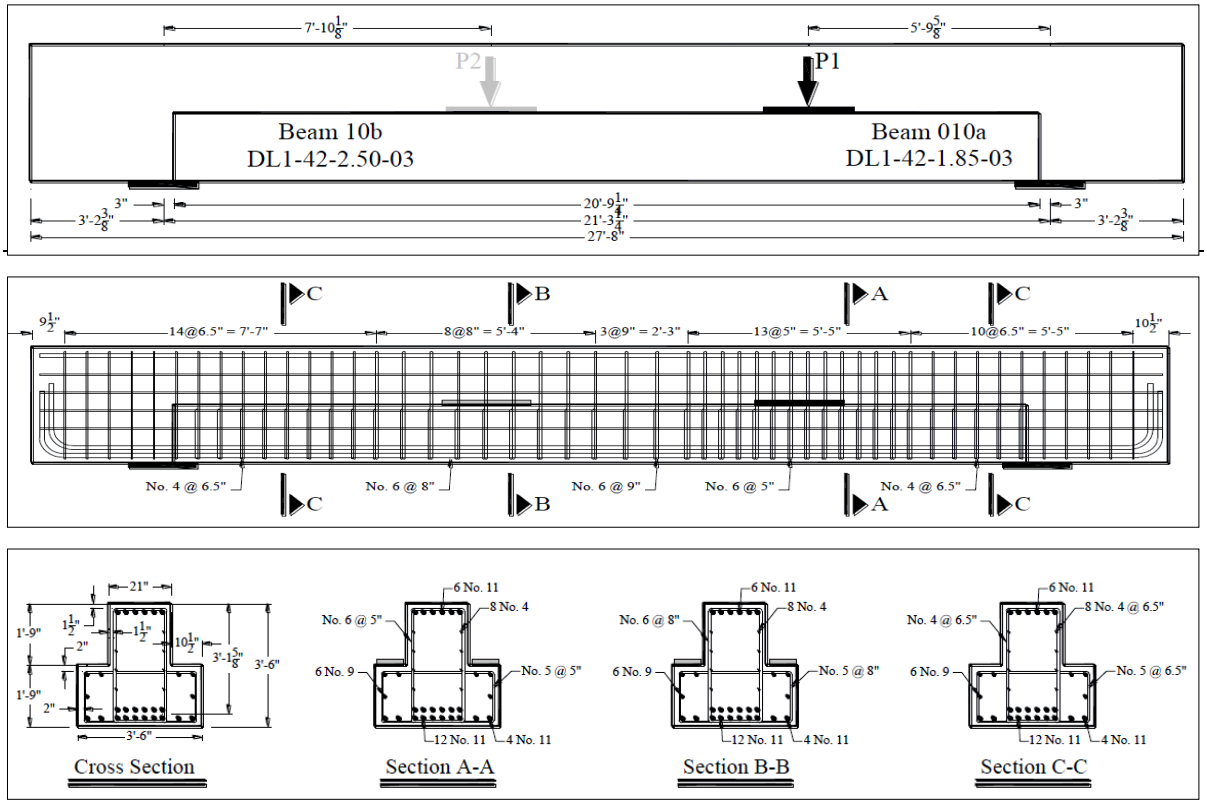

Figure 20. Concrete dimensions and reinforcement details of the specimen

The results showed a good agreement with the FE model as shown in Figure 21. The figure shows that there was only a 9% difference in the ultimate capacity between the theoretical and the experimental models.

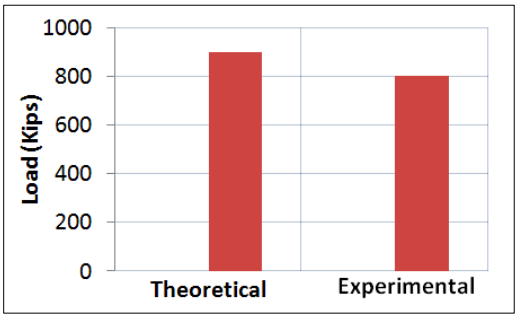

Figure 21. Ultimate load of the theoretical model vs. the experimental model

The mode of failure of specimen DL1-42-2.50-03 was web shear. The direct strut was crushed after applying the total load. Figures 22 and 23 show the crack pattern obtained from the experiment and the plastic strain from the finite element analysis of specimen DL1-42-2.50-03.

Figure 22. Crack pattern at ultimate load of specimen DL1-42-2.50-03

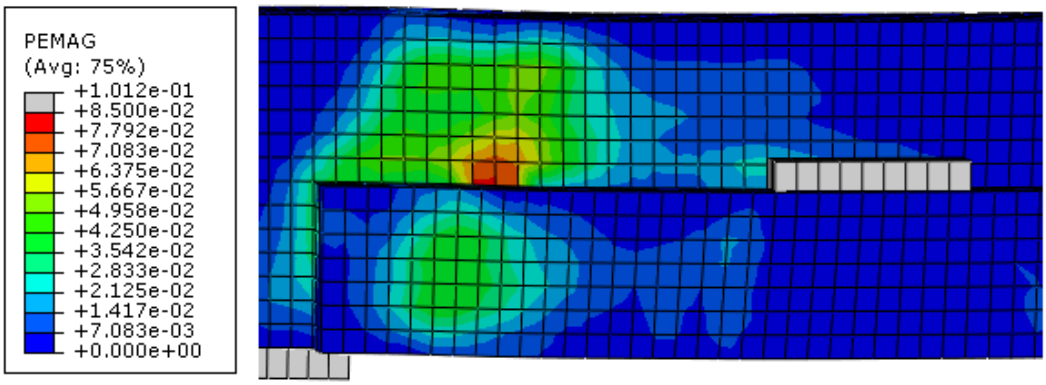

Figure 23. FEM plastic strain of specimen DL1-42-2.50-03

5. Model Validation

The developed FE model was validated using the results of the experimental program shown in Figure 14. The values of concrete compressive strength and steel reinforcement yield strength defined previously in the material clause and Table 2 were used as input in the FEM. The load-deflection curves derived from the FEM were compared with those obtained from the experimental program, as illustrated in Figure 24.

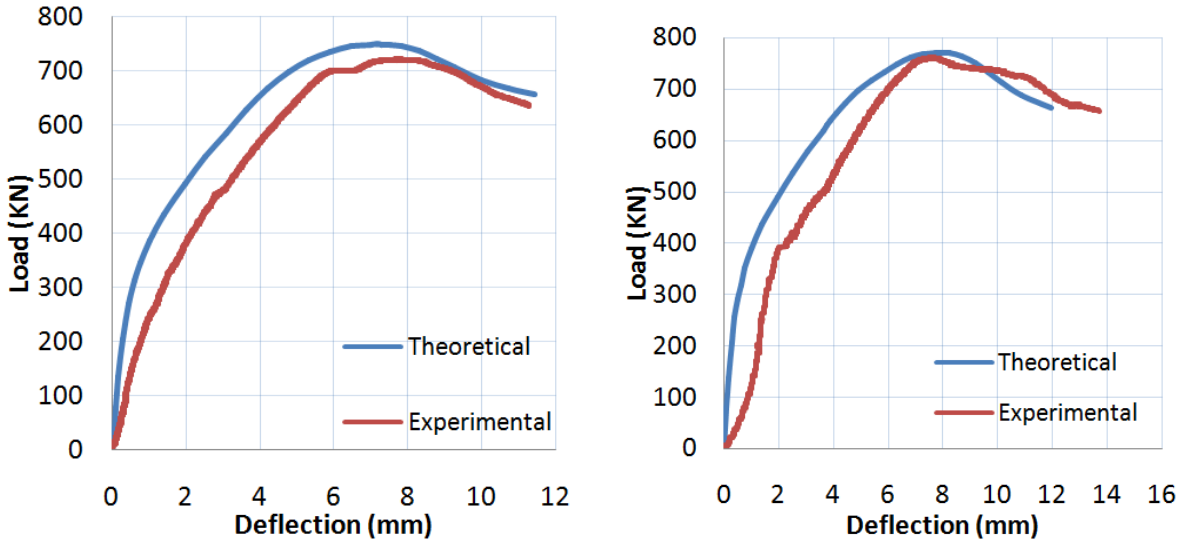

(a) IDB1

(b) IDB2

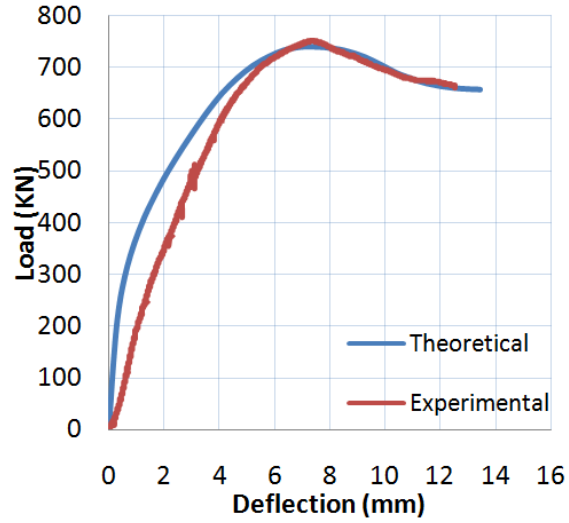

(c) IDB3

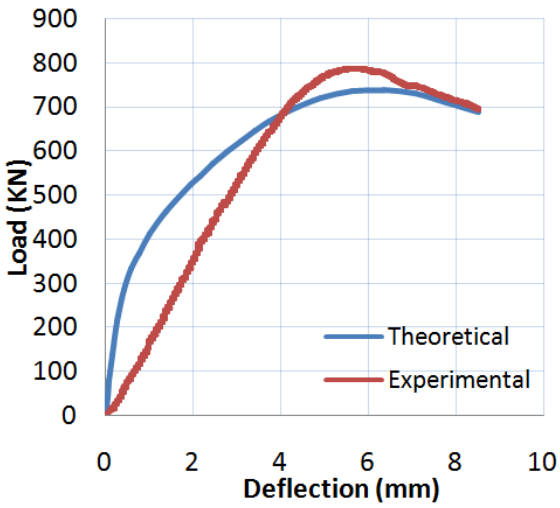

(d) IDB4

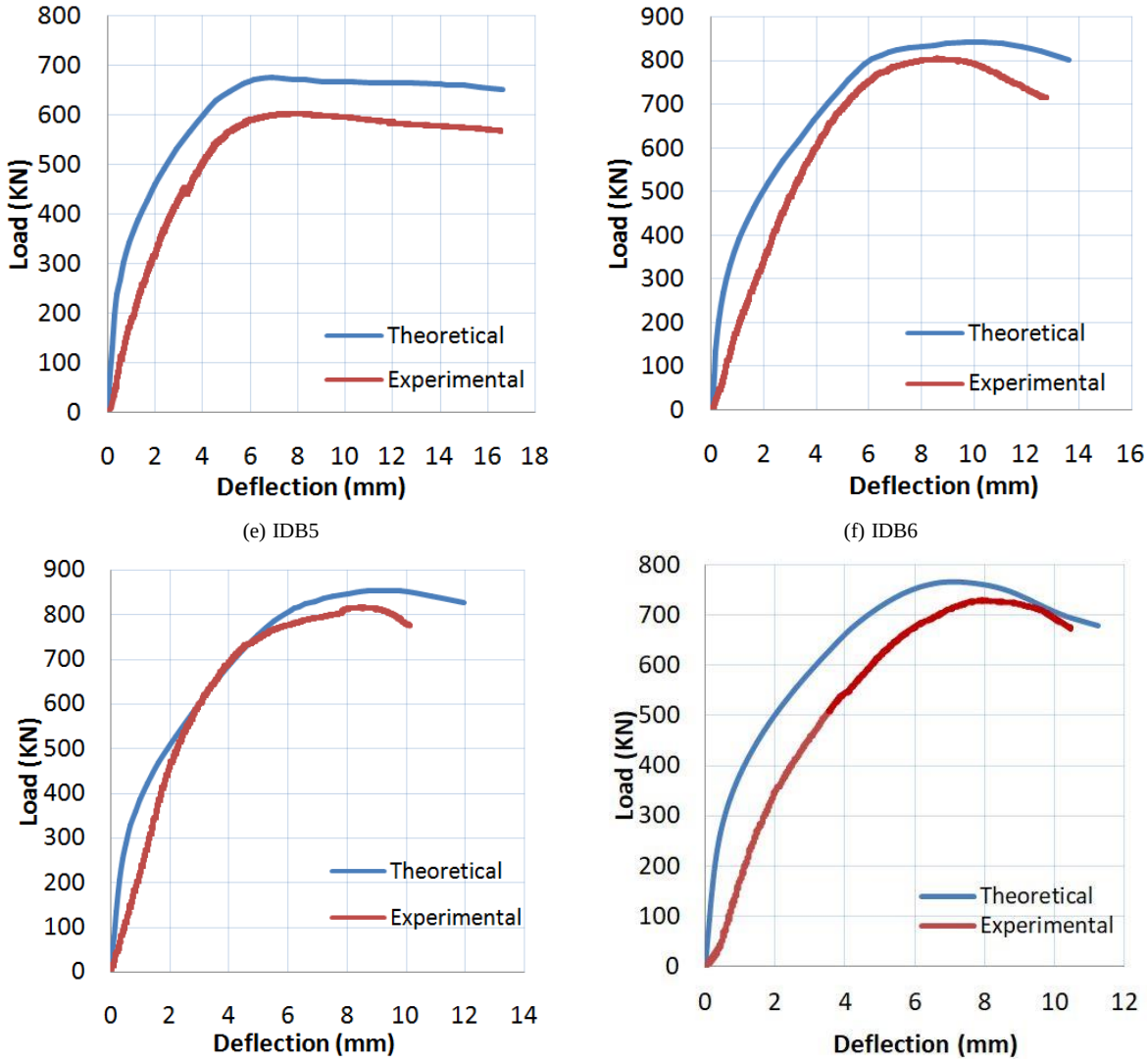

(e) IDB5 (f) IDB6

(g) IDB7 (h) IDB8

Figure 24. Load-deflection curves-experimental vs. FEM

The difference between the maximum load of the experimental program and FEM ranges between 3% to 7% in all specimens except IDB 5, where the difference was 10%. This difference is attributed to many factors, which can be summarized as follows: the properties and constitutive behavior of the material used in the theoretical model are not the same as the actual values. Table 5 shows the test ultimate load versus the ultimate load calculated using the FE model.

Table 5. Test ultimate load vs. the calculated ultimate load

Specimen no.	$P_{u\ Test}$(kN)	$P_{u\ Calc}$ (kN)	$P_{u\ Calc}$/ $P_{u\ Test}$
IDB1	729.9	749.1	1.03
IDB2	750.5	771.3	1.03
IDB3	761.3	741.0	0.97
IDB4	796.6	739.0	0.93
IDB5	612.2	675.2	1.10
IDB6	814.3	842.3	1.03
IDB7	825.1	852.3	1.03
IDB8	738.8	765.9	1.04
Standard Deviation		**0.051**	
Coefficient of variation		**0.05**	

The first crack load predicted by the numerical model is greater than that obtained from the experimental program; this could be because of the difference between the used post-peak tension softening curve of concrete and the actual behavior. The contact surface between the loading and supporting plates and the concrete beam was modeled as a complete bond, which is not an accurate representation, as is the relationship between the concrete and reinforcement

bars. Moreover, the results could be affected by the rate of loading. Also, the experimental results are affected by imperfections and defects in the materials. The modeled response confirms that the chosen model can accurately represent the beam's behavior up to failure and exhibits good agreement with the experimental findings. The model yielded accurate estimates of strength with a minimum $Pu_{calc}/P_{u\ Test}$ value of 0.93, a maximum of 1.10, an average of 1.02, and a coefficient of variation of 0.05 for the inverted-T deep beams, as presented in Table 5. The verified model can be used to predict the behavior of IT deep beams. Figure 25 shows the plastic strain extracted from the FEM. The results of the plastic strain also showed a close behavior to the cracks of the tested specimens.

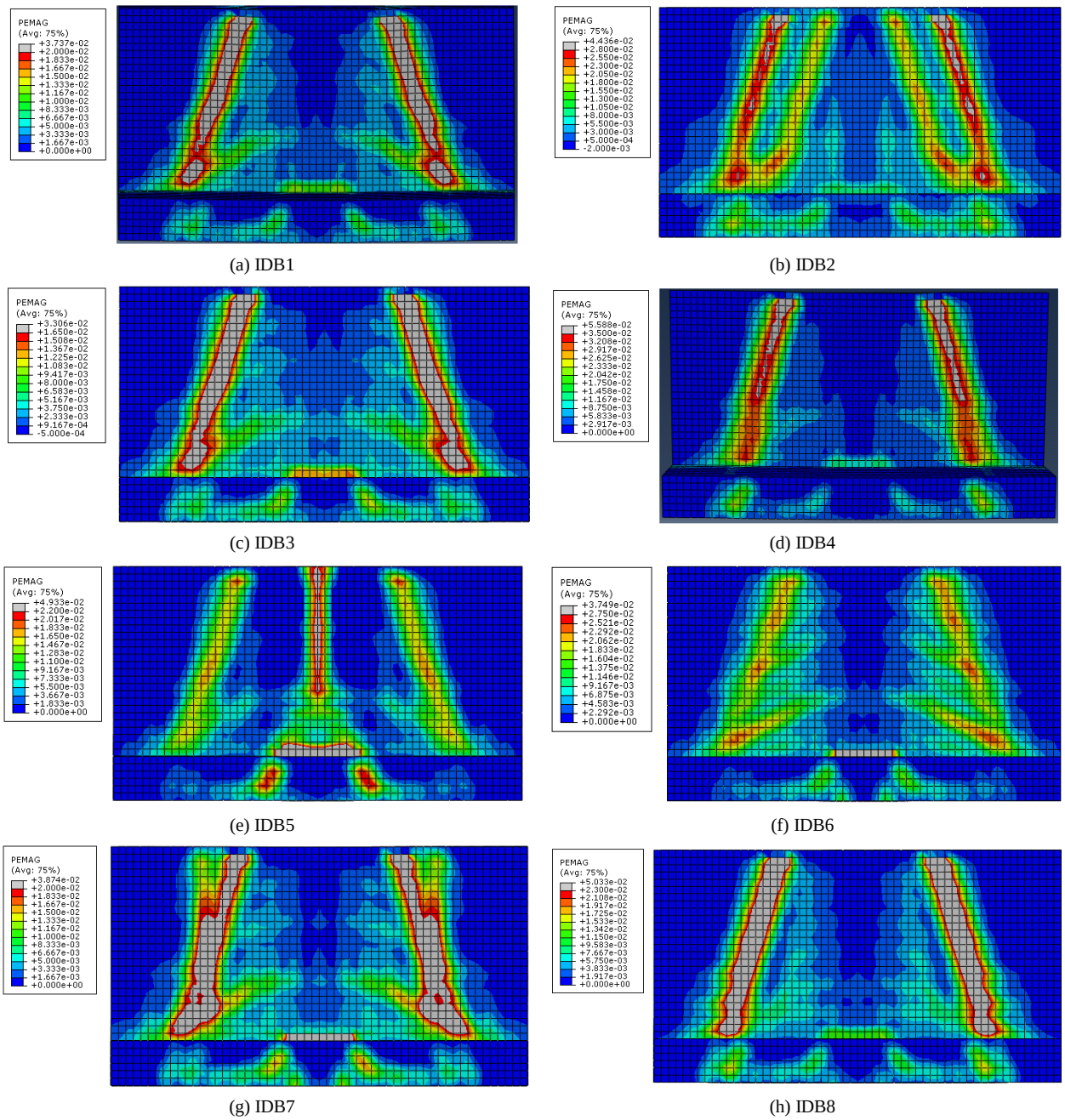

Figure 25. ABAQUS plastic strain

6. Comparison with Design Codes

Inverted-T deep beams typically experience complicated states of stress along most of their spans. The disturbed stress zones are generated due to the application of concentrated loads and reactions. Sectional design is not applicable in disturbed zones. Codes specify separate design provisions for the web and ledge portions of the inverted-T deep beam. For the web portion, if the shear span-to-depth ratio is less than about 2.0, strut-and-tie modeling should be considered. For the ledge portion, beam ledges may be designed using the strut-and-tie model or the empirical method described in clauses 5.13.2.5.2 through 5.13.2.5.5 of the AASHTO code [17]. The AASHTO empirical method is based on designing the beam ledge to prevent potential failure modes (shear, flexure, punching, and bearing) and fulfill reinforcement requirements.

The ultimate capacities obtained from the test results were compared with the preliminary capacities calculated by using the theoretical methods of the relevant codes: ECP 203-2020 [1], ACI 318-19 [2], and AASHTO-2020 [17]. A big difference was found between the beam capacity of the experimental results and the design codes' methods, as shown in Tables 6 and 7. The results of the experimental program exceeded the codes' results by about 2 to 3 times. It is noteworthy that when using the STM method shown in Table 6, the web governed the beam capacity in all codes. Also, the ECP code resulted in the most conservative beam capacity. While in the AASHTO empirical method shown in Table 7, punching was the critical mode of failure in all codes, and the AASHTO resulted in the most conservative beam capacity.

Table 6. Test ultimate load vs. ultimate load using AASHTO Empirical Method

Modes of Failure	ECP 203-2020 (kN)	ACI 318-19 (kN)	AASHTO-2020 (kN)
Shear between ledge and web	851.4	696.1	696.1
Bearing at loading plate	1000.0	1550.4	1550.4
Bearing at support plate	458.3	465.0	465.0
Punching of the ledge under the load	373.8	351.0	347.3

Table 7. Test ultimate load vs. ultimate load using STM method

Specimen no.	$P_{u\ Test}$ (KN)	ECP 203-2020 (kN)		ACI 318-19 (kN)		AASHTO-2020 (kN)	
		Web Capacity	Ledge Capacity	Web Capacity	Ledge Capacity	Web Capacity	Ledge Capacity
IDB1	729.9	286.5	438.5	312.9	476.8	319.8	485.6
IDB2	750.5						
IDB3	761.3						
IDB4	796.6						
IDB5	612.2						
IDB6	814.3						
IDB7	825.1						
IDB8	738.8						

Moreover, as the impact of reinforcement change is not considered in the analytical methods, only a single value for the beam capacity is calculated for the eight specimens. In inverted-T deep beams with long ledges [15], the diagonal struts are restricted by the width of the web on the upper part of the web but not in the lower part, where stresses can spread along the ledge width near the support node, as shown in Figure 26. In such a case, the strut's weakest point may shift from the strut-to-node interface to the position where the thickness of the strut varies from the ledge width to the web width. As a result, the thickness of the strut-to-node interface at the support may be defined as the smallest of the bearing width and the web thickness.

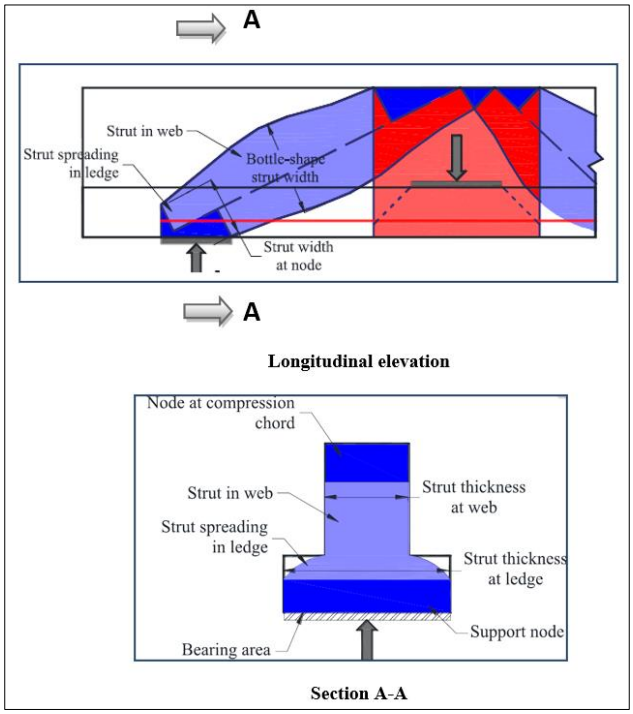

Figure 26. Width variation in bottle-shape struts

The IT deep beam capacity was recalculated at the location of sections A-A, as the strut width is larger. As shown in Table 8, the capacity of the beam was found to be higher than the values presented in Table 6 by about 23%. However, the values are still much lower than the results obtained from the tested specimens.

Table 6. Test ultimate load vs. ultimate load using STM method at section A-A

Specimen no.	$P_{u\ Test}$ (KN)	ECP 203-2020 (kN)	ACI 318-19 (kN)	AASHTO-2020 (kN)
		Web Capacity		
IDB1	729.9	354.1	385.5	394.4
IDB2	750.5			
IDB3	761.3			
IDB4	796.6			
IDB5	612.2			
IDB6	814.3			
IDB7	825.1			
IDB8	738.8			

The previous comparison with the various methods of analysis of IT deep beams included in the relevant design codes showed a significant difference between the codes' estimation and test results, so the codes' limitations need to be studied through an extensive parametric study and more reasonable design criteria need to be proposed.

7. Comparison between IT with Long and Short Ledge using the FEM

Based on the proposed FE model using ABAQUS [20], IDB1 was re-modeled with ledges of types 2 and 3. These types of ledges were studied in previous research [15, 16], as mentioned before in the literature review, while the beams with ledges of type 4 were not studied. Figure 27 shows the principal stresses and the load-deflection curves of the three types of ledges. The results of the FEM model showed that the IT deep beam with a long ledge (type 4) can sustain a load higher than that of beams of ledges types 2 and 3 by about 32% and 56%, respectively. It can be seen in Figure 27a that the behavior was based on the arch action, and the load was completely transferred to the support through the compression struts. In Figures 27b and 27c, the beam behavior was a combination of the arch and beam actions. A theoretical method combining both arch and beam action is needed to determine the actual capacity of beams with long ledges.

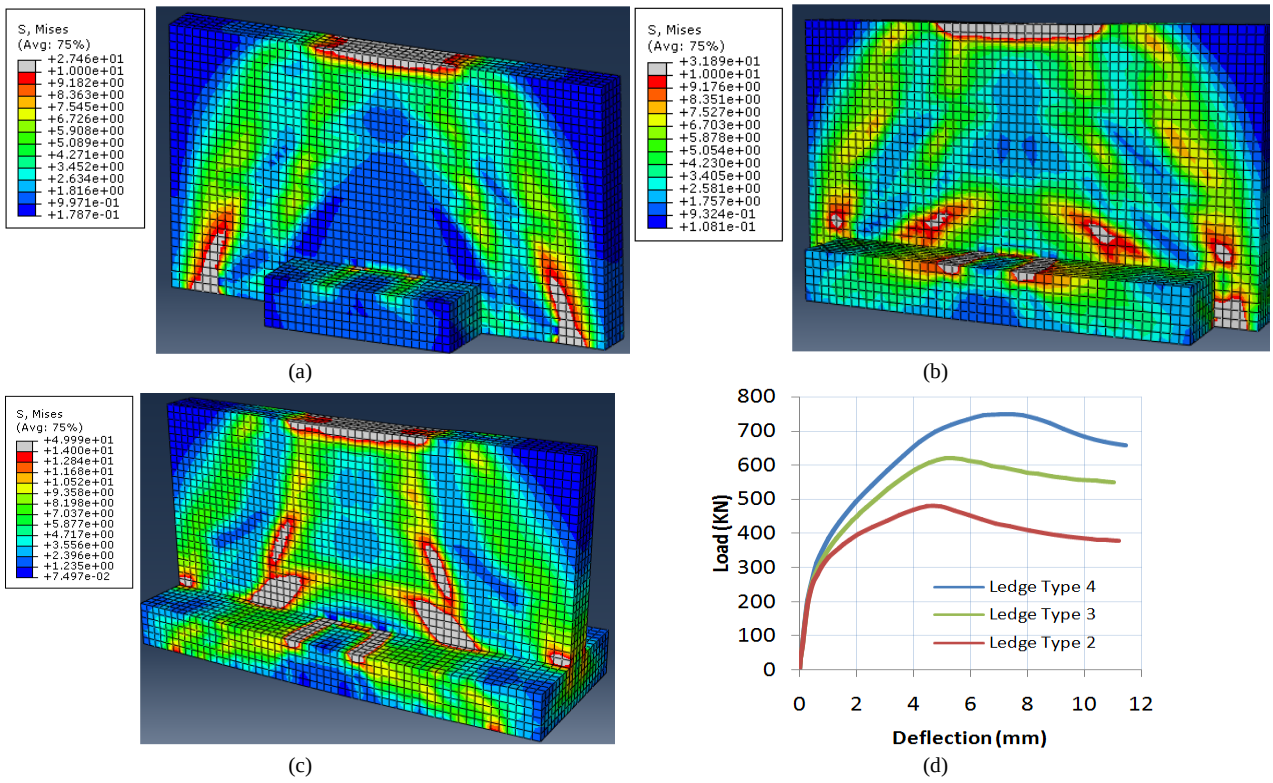

Figure 27. (a) Stress distribution in ledge IT deep beam with ledge type 2, (b) Stress distribution in ledge IT deep beam with ledge type 3 (c) Stress distribution in ledge IT deep beam with ledge type 4, (d) Load-deflection curve of IT deep beam with ledges of type 2, 3, and 4.

8. Conclusions

The behavior of IT deep beams was investigated in this study through an experimental program comprised of eight specimens. Both hanger and web shear reinforcements were investigated to examine their effect on the behavior of IT deep beams. A finite element model was generated by using ABAQUS software to extensively study the behavior of IT deep beams. To check the codes' methods of analysis, the ultimate capacities obtained from the test results were compared with the preliminary capacities calculated by using the theoretical methods of the relevant codes. The following list provides a summary of the conclusions:

- Changing the bar diameter of the hanger reinforcement while keeping almost the same reinforcement area has an insignificant effect on the beam capacity.
- Changing the hanger reinforcement arrangement by increasing hanger reinforcement spacing, as in IDB5, where only one hanger was passing through the plate region, reduced the arch action of the beam. The flexural behavior becomes more dominant, causing a noticeable reduction in capacity by more than 20%. The maximum spacing for hanger reinforcement needs to be determined to ensure complete load transmission to the web. The maximum spacing will be studied in the parametric study.
- Changing the hanger reinforcement arrangement by concentrating the hanger reinforcement only at the loading plate distance in IDB2 without applying the 45-degree concept of load spreading (W+2df) didn't affect the capacity of the IT deep beam. This output indicates that the hanger reinforcement could be concentrated at a distance less than (W+2df) and the beam still achieves the same ultimate capacity.
- Increasing the hanger reinforcement ratio increased the beam stiffness after the formation of the first diagonal crack, resulting in a reduction of 15.5% in the mid-span deflection and an increase in the capacity of 6.5%.
- Increasing the vertical web reinforcement ratio increases the ultimate capacity of the IT deep beam significantly. However, decreasing web reinforcement spacing was more efficient than increasing the bar diameter. Vertical web reinforcement intersecting struts needs to be considered when calculating strut capacity, not only the reinforcement aligned in the direction of the struts and confined by stirrups as recommended in the design codes.
- Increasing the horizontal web reinforcement ratio has a small effect on the capacity of IT deep beams.
- The developed nonlinear finite element ABAQUS model was able to capture the response of all the tested specimens. In particular, the model was capable of properly modeling the load-deformation response, crack patterns, and ultimate capacity of the beams.
- The ultimate capacity of an IT deep beam with a long ledge is much higher than that of a short ledge; hence, it is recommended to use an IT deep beam with a long ledge to utilize the maximum capacity.

Future Study:

An extensive parametric study is conducted and will be presented in a following research article where the following topics will be studied:

- The effect of span-to-depth ratio (L/d) on the behavior of the IT deep beam and obtaining L/d values at which the IT beam behavior changes from deep to slender beam. Furthermore, an extensive study for ledge dimensions (length, depth, and width), longitudinal reinforcement, and ledge reinforcement will be included.
- The analysis of the IT deep beam using design codes, either the Strut and Tie method or AASHTO LRFD Bridge Design Specifications, showed a significant difference with the test results, hence, these methods will be verified based on the experimental program results, and a modified numerical analysis model will be proposed through the extensive parametric study and based on more reasonable design criteria. The effects of the long ledge, the hanger, and the web shear reinforcement shall be included in these methods.
- Strengthening the ledge in the region under the load plate to prevent punching failure by adding stirrups, bent bars, or steel plates in this region needs to be studied.
- A comparison between the ultimate capacity of the IT deep beam and the top-loaded deep beam will also be presented in the parametric study.

9. Declarations

9.1. Author Contributions

Conceptualization, H.S., R.T.S.M., and A.T.; methodology, H.S., R.T.S.M., and A.T.; software, H.S.; investigation, H.S.; writing—original draft preparation, H.S. and R.T.S.M.; writing—review and editing, H.S., R.T.S.M., and A.T.; supervision, R.T.S.M. and A.T. All authors have read and agreed to the published version of the manuscript.

9.2. Data Availability Statement

The data presented in this study are available in the article.

9.3. Funding

The authors received no financial support for the research, authorship, and/or publication of this article.

9.4. Conflicts of Interest

The authors declare no conflict of interest.

10. References

[1] ECP-203-2020. (2020). The Egyptian Code for Design and Construction of Concrete Structures. Housing and Building Research Center, Cairo, Egypt.

[2] ACI 318-19. (2019). Building Code Requirements for Structural Concrete and Commentary. American Concrete Institute (ACI), Michigan, United States. doi:10.14359/51716937.

[3] EN 1992-1-1 (2004). Eurocode 2: Design of concrete structures (Part 1-1): General rules and rules for buildings. European Committee for Standardization (CEN), Brussels, Belgium.

[4] Graf, O., Brenner, E., & Bay, H. (1943). Experiments with a wall-like girder made of reinforced concrete. Deutscher Ausschuss Fur Stahlbeton, 99, 41–54. (In German).

[5] Leonhardt, F. (1966). Wall-like beams, German Committee for Reinforced Concrete. Reinforced Concrete Structures. (In German).

[6] Furlong, R. W., Ferguson, P. M., & Ma, J. S. (1971). Shear and anchorage study of reinforcement in inverted T-beam bent cap girders. Research Project No. 113-4, Center for Highway Research, University of Texas, Austin, United States.

[7] Mirza, S. A., Furlong, R. W., & Ma, J. S. (1988). Flexural Shear and Ledge Reinforcement in Reinforced Concrete Inverted T-Girders. ACI Structural Journal, 85(5), 509–520. doi:10.14359/2790.

[8] Furlong, R. W., & Mirza, S. A. (1974). Strength and serviceability of inverted T-beam caps subject to combined flexure, shear, and torsion. No. FHWA-RD-75-S0401 Final Report, Texas State Department of Highways & Public Transport, Austin, United States.

[9] Mirza, S. A., & Furlong, R. W. (1985). Design of Reinforced and Prestressed Concrete Inverted T Beams for Bridge Structures. Journal - Prestressed Concrete Institute, 30(4), 112–136. doi:10.15554/pcij.07011985.112.136.

[10] Smith, K. N., & Fereig, S. M. (1974). Effect of Loading and Supporting Conditions on the Shear Strength of Deep Beams. Special Publication, 42, 441-460.

[11] Fereig, S. M., & Smith, K. N. (1977). Indirect Loading on Beams with Short Shear Spans. Journal of the American Concrete Institute, 74(5), 220–222. doi:10.14359/11005.

[12] Cusens, A. R., & Besser, I. I. (1985). Shear Strength of Reinforced Concrete Wall-Beams Under Combined Top and Bottom Loads. Structural Engineer, 63 B(3), 50–56.

[13] Tan, K. H., Kong, F. K., & Weng, L. W. (1997). High strength concrete deep beams subjected to combined top-and bottom-loading. Structural Engineer, 75(11), 191–197.

[14] CIRIA Guide 2. (1977). Design of Deep Beams in Reinforced Concrete. Ove Arup and Partners, Construction Industry Research and Information Association, London, United Kingdom.

[15] Fernandez Gomez, E. (2012). Design Criteria for Strength and Serviceability of Inverted-T Straddle Bent Caps. Ph.D. Thesis, University of Texas, Austin, United States.

[16] Varney, N. L., Fernández-Gómez, E., Garber, D. B., Ghannoum, W. M., & Bayrak, O. (2015). Inverted-T beams: Experiments and strut-and-tie modeling. ACI Structural Journal, 112(2), 147–156. doi:10.14359/51687403.

[17] AASHTO. (2020). AASHTO LRFD Bridge Design Specifications. American Association of State Highway and Transportation Officials, Washington, United States.

[18] Garber, D. B., Varney, N. L., Fernández Gómez, E., & Bayrak, O. (2017). Performance of ledges in inverted-T beams. ACI Materials Journal, 114(2), 487–498. doi:10.14359/51689451.

[19] Rai, P. (2021). Non-Linear Finite Element Analysis of RC Deep Beam Using CDP Model. Advances in Technology Innovation, 6(1), 01–10. doi:10.46604/aiti.2021.5407.

[20] ABAQUS. (2017). SIMULIA User Assistance 2017, Dassault Systems Similia Corp. ABAQUS, Johnston, United States.

[21] Ali, Y. A., Assi, L. N., Abas, H., Taresh, H. R., Dang, C. N., & Ghahari, S. A. (2023). Numerical Investigation on Effect of Opening Ratio on Structural Performance of Reinforced Concrete Deep Beam Reinforced with CFRP Enhancements. Infrastructures, 8(1), 2. doi:10.3390/infrastructures8010002.

[22] ASTM C150/C150M-18. (2019). Standard Specification for Portland Cement. ASTM International, Pennsylvania, United States. doi:10.1520/C0150_C0150M-18.

[23] ASTM C33/C33M-18. (2018). Standard Specification for Concrete Aggregates. ASTM International, Pennsylvania, United States. doi:10.1520/C0033_C0033M-18.

[24] Birrcher, D., Tuchscherer, R., Huizinga, M., Bayrak, O., Wood, S. L., & Jirsa, J. O. (2009). Strength and serviceability design of reinforced concrete deep beams. No. FHWA/TX-09/0-5253-1, Center for Transportation Research, University of Texas, Austin, United States.

[25] Walraven, J. C., & Bigaj-van Vliet, A. (2011). The 2010 fib Model Code for Structural Concrete: a new approach to structural engineering. Structural Concrete, 12(3), 139-147. doi:10.1002/suco.201100025.